Preparation and Characterization of Nano-galvanic Bimetallic Fe/Sn Nanoparticles Deposited on Talc and its Enhanced Performance in Cr(VI) Removal

Mitra Bayat
Amirkabir University of Technology
Bahram Nasernejad (banana@aut.ac.ir)
Amirkabir University of Technology
Cavus Falamaki
Amirkabir University of Technology

Research Article

Keywords: nanoscale zero-valent iron, clay-supported nanoparticle, bimetallic nanoparticle, chromium removal, water remediation

Posted Date: February 4th, 2021

DOI: https://doi.org/10.21203/rs.3.rs-154332/v1

Version of Record: A version of this preprint was published at Scientific Reports on April 8th, 2021. See the published version at https://doi.org/10.1038/s41598-021-87106-0.

Preparation and characterization of nano-galvanic bimetallic Fe/Sn nanoparticles deposited on talc and its enhanced performance in Cr(VI) removal

Mitra Bayat, Bahram Nasernejad*, Cavus Falamaki

Department of Chemical Engineering, Amirkabir University of Technology, Tehran, 15875-4413, Iran

*Corresponding author: Department of Chemical Engineering, Amirkabir University of Technology, Tehran, 15875-4413, Iran

E-mail address: banana@aut.ac.ir (B. Nasernejad)

Phone number: +982164543291

Abstract

In this study, talc-supported nano-galvanic nZVI/Sn bimetallic particles was successfully synthesized and utilized for Cr(VI) remediation. Talc-nZVI/Sn nanoparticles were characterized by SEM, EDS, FTIR, XRD, zeta potential, and BET analysis. The findings verified the uniform dispersion of nZVI/Sn nanoparticles on talc surface. The formation of numerous nano-galvanic cells between nZVI core and Sn shell enhanced the potential of bimetallic particles in Cr(VI) mitigation. Batch experiments were carried out to investigate optimum conditions and total Cr(VI) removal was achieved in 20 minutes using Sn/Fe mass ratio of 6/1, the adsorbent dosage of 2 g/L, initial Cr(VI) concentration of 80 mg/L, at the acidic environment (pH=5) and temperature of 303 K. Besides, co-existing of metallic cations turned out to facilitate the electron transfer from the nano-galvanic couple of NZVI/Sn and suggested the revolution of bimetallic particles to trimetallic composites. The aging study of the nanocomposite confirmed its constant high activity during 60 days. The removal reaction was well described by the pseudo-second-order kinetic and the Langmuir isotherm models. Overall, due to the synergistic galvanic cell effect of nZVI/Sn nanoparticles and full coverage of active sites by Sn layer, Talc-nZVI/6Sn was utilized as a promising nanocomposite for fast and highly efficient Cr(VI) elimination.

Keywords: nanoscale zero-valent iron, clay-supported nanoparticle, bimetallic nanoparticle, chromium removal, water remediation

Introduction

With the rapid development of industrial activities, large amount of heavy metals has been transferred into the natural environment, and their continuous accumulation and high permeability have posed great threats to living organisms and environment safety [1,2]. The toxicity or carcinogenicity of heavy metal ions, such as Cr(VI), Pb(II), Cd(II), Cu(II), Zn(II), Hg(II), and Ni(II) can cause long-term damage to humans and other species [3].

Chromium mainly exist in two oxidation states of Cr(VI) and (III) among which Cr(VI) is 100 times more toxic than Cr(III). Cr(VI) has been classified as priority controlled contaminant and could cause cancers and respiratory diseases in case of excessive exposure [4,5]. On the other hand, Cr(III) is significantly less toxic and even an essential nutrient for humans and living organisms at trace levels. Due to low aqueous solubility and subsequent low mobility of Cr(III), the reduction of Cr(VI) to Cr(III), followed by in-situ Cr(III) adsorption or precipitation has been the most suitable approach to mitigate Cr(VI) pollution (Fu et al., 2015b; Kadu and Chikate, 2013; Vilardi et al., 2018; Zhu et al., 2016). Consequently, the employment of the improved treatment technology for fast and complete Cr(VI) reduction has drawn lots of attention [10–13].

Technologies based on adsorption techniques have been known as adequate and straightforward approaches for Cr(VI) elimination, due to their wide adaptability and cost-effectiveness [14,15]. Among different adsorbent for heavy metal remediation, nanoscale zero-valent iron (nZVI) particles which have combined large specific surface area, high reactivity, abundant surface binding sites, low toxicity, and absence of secondary pollution, has been proved as an efficient and environmental-friendly materials. In recent years, nZVI has emerged as a promising material Cr(VI) remediation from aqueous solutions [16–18].

Regardless of their high efficiency in the removal of contaminants, nZVI has faced some limitations, including instability, strong tendency for agglomeration, and rapid oxidation. To

address these issues, different modifications such as metal doping, coating the surface of nZVI, or immobilization of nZVI onto support are applied [19,20]. The wide availability, cost-effectiveness and long-term stability of clay minerals (e.g., montmorillonite, kaolinite, Bentonite, talc) have introduced them as great supporting materials for nZVI particles (Ezzatahmadi et al., 2017; Fu et al., 2015b; Wang et al., 2014; Wu et al., 2015; Yadav et al., 2019; Zhao et al., 2019).

Besides utilizing the preferences of clay-supported nZVI particles, the reactivity of nZVI particles has been enhanced by the deposition of a layer of other metals (e.g., Pd, Ni, Cu) onto nZVI surfaces [10,24–26]. The addition of other metals would provide hydrogen catalysts or reactive electron donors and would lead to the enhanced properties of bimetallic particles, including slower passivation of Fe^0 surface and faster reaction kinetics [27]. Besides, bimetallic nanoparticles could form a lot of nano-galvanic couples which speeded up the electron transfer of galvanic corrosion. Despite the enhanced performance, the wide application of bimetallic particles has been limited due to the high expense of the coated metals. In this regard, the application of a low-cost and efficient metal would be an advantageous approach [24].

clay-supported iron based bimetallic nanoparticles, which have combined both advantages of supported and coated nanoparticles, have proved great potential in heavy metals elimination [27–29]. Despite their effectiveness in heavy metal removal, only little researches have been conducted using limited kind of clays (mainly kaolinite and montmorillonite) and metals (Ni, Pd). Talc with the chemical formula of $Mg_3Si_4O_{10}(OH)_2$ is one of the non-ionic clays with a 2:1 structure, which is composed of a sheet of magnesium hydroxide ($MgO.H_2O$) located among two sheets of silicate (SiO_2) layers. Although showing high performance as supporting material for nanoparticles, talc has been studied intensively [30,31].

To the best of our knowledge, the application of nanocomposites containing talc as supporting surface and tin as a coating material for Cr(VI) remediation has not been reported to date. Herein, novel talc-supported nano-galvanic Fe/Sn bimetallic nanoparticles (Talc-nZVI/Sn) was prepared and used to investigate the Cr(VI) remediation from aqueous solution. A two-step synthesis technique was employed to achieve core-shell bimetallic nanoparticles deposited on talc. The removal of Cr(VI) was compared using talc, and talc-supported nZVI/Sn with varying Sn/Fe ratios. In addition, the effects of various environmental conditions such as initial Cr(VI) concentration, Talc-nZVI/Sn dosage, initial pH, and temperature on Cr(VI) removal were evaluated. The influence of co-existing of different metallic cation in Cr(VI) aqueous solution on the galvanic cells performance was investigated. Moreover, the reusability and aging study of the Talc-nZVI/Sn particles were investigated. Finally, the adsorption kinetics, adsorption isotherm, and reaction mechanism of Cr(VI) removal using Talc-nZVI/Sn were studied.

Results and discussion

Characterizations

The morphology and surface structure of different materials, including talc, Talc-nZVI/1Sn, Talc-nZVI/4Sn, and Talc-nZVI/6Sn before and after reaction with Cr(VI) were analyzed by SEM (Fig. 1). Talc (Fig. 1(a)) is characterized by its smooth surface and layered structure. The SEM images of the synthesized nanoparticles of Talc-nZVI/1Sn, Talc-nZVI/4Sn, and Talc-nZVI/6Sn, displayed approximately spherical particles, with a size of 30 to 200 nm, which are uniformly dispersed on the talc surface. Also, with an increase of the Sn/Fe mass ratio from 1 to 6, some changes in average particle size were seen. Particles in Talc-nZVI/1Sn were mainly in the range of 30 to 100 nm, but with increasing the Sn/Fe mass ratio, slightly larger particles were observed, so that Talc-nZVI/6Sn exhibited particles in the

range of 50-200 nm. The bigger particles in Talc-nZVI/6Sn compared to Talc-nZVI/1Sn were ascribed to the increased loading of Sn, which created a thicker shell layer on nZVI cores.

Fig. 1(d) and 1(e) display the changes in the morphology of Talc-nZVI/6Sn before and after Cr(VI) removal. The unreacted Talc-nZVI/6Sn showed particles with their explicit borders, while the reacted composite exhibited a porous surface. This difference in surface structure could be attributed to the reaction precipitates which settled on the outer surface of nanoparticles and within pores of talc structure. Also, this is confirmed by the EDS elemental mapping of chromium on Talc-nZVI/6Sn after Cr(VI) removal (Fig. 2(d)).

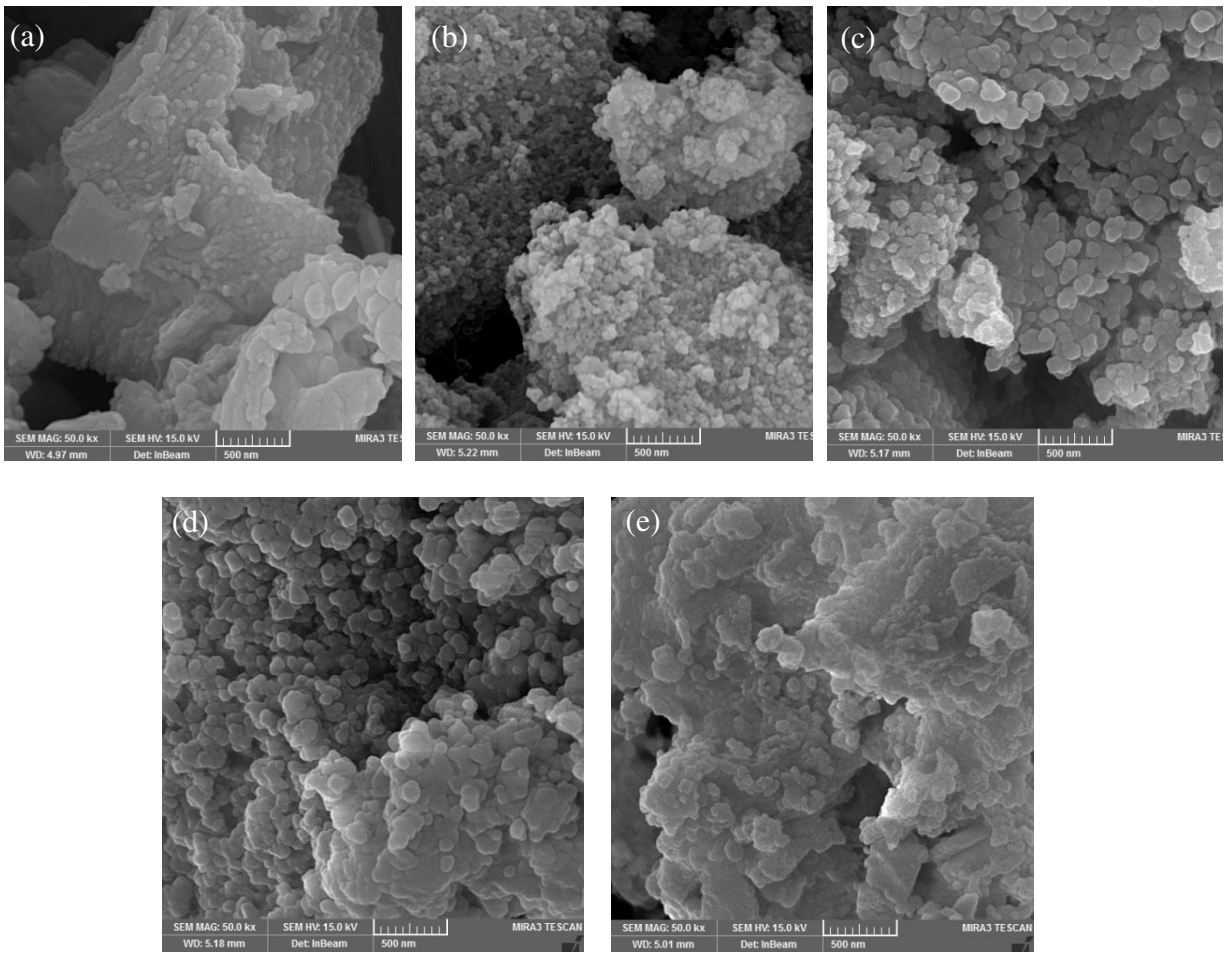

Fig. 1. SEM images of (a) talc (b) Talc-nZVI/1Sn (c) Talc-nZVI/4Sn (d) Talc-nZVI/6Sn (e) Talc-nZVI/6Sn after reaction with Cr(VI)

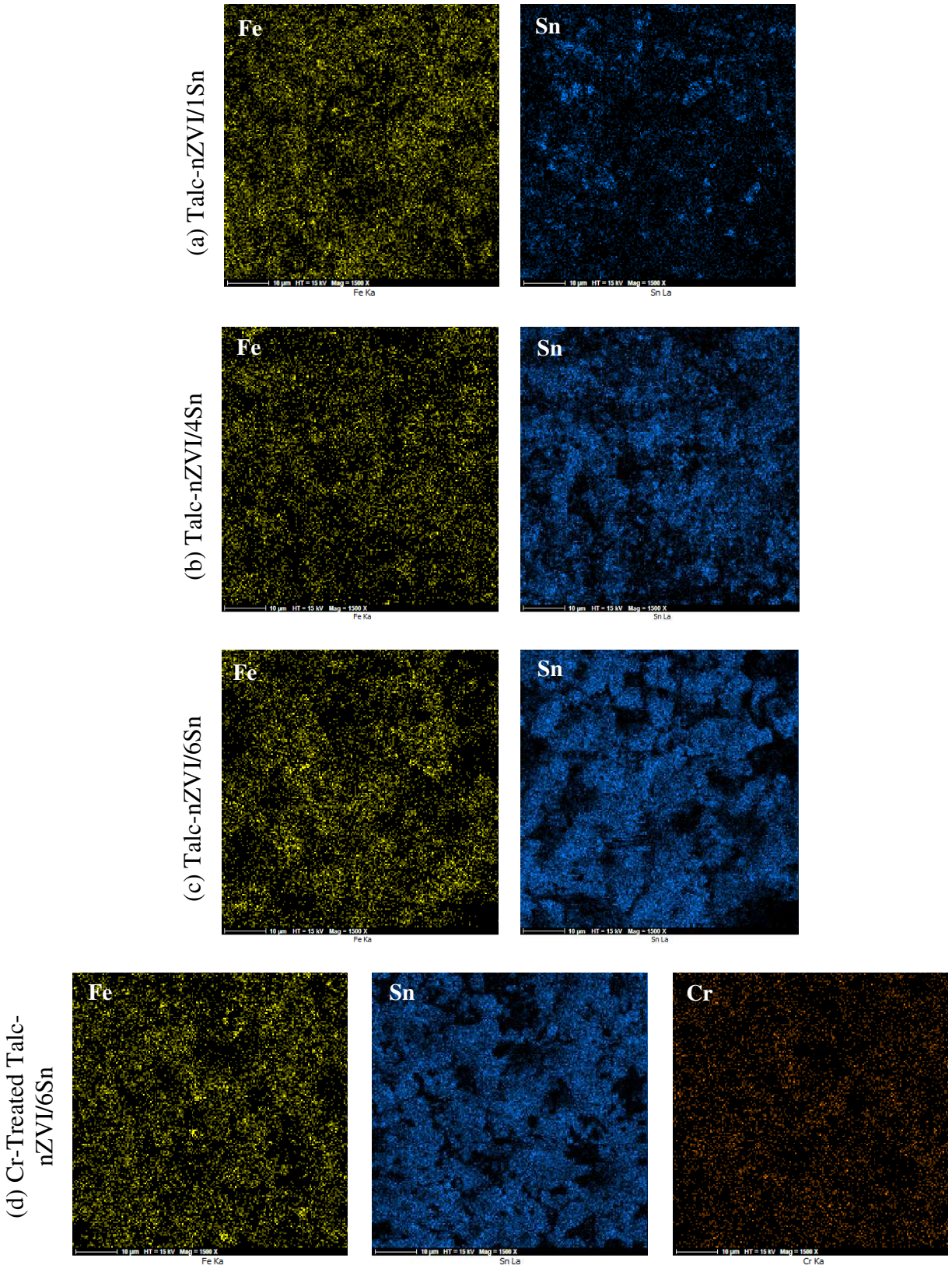

Fig. 2. EDS mapping of the analyzed area; iron and tin in (a) Talc-nZVI/1Sn (b) Talc-nZVI/4Sn (c) fresh Talc-nZVI/6Sn and (d) Cr-treated Talc-nZVI/6Sn

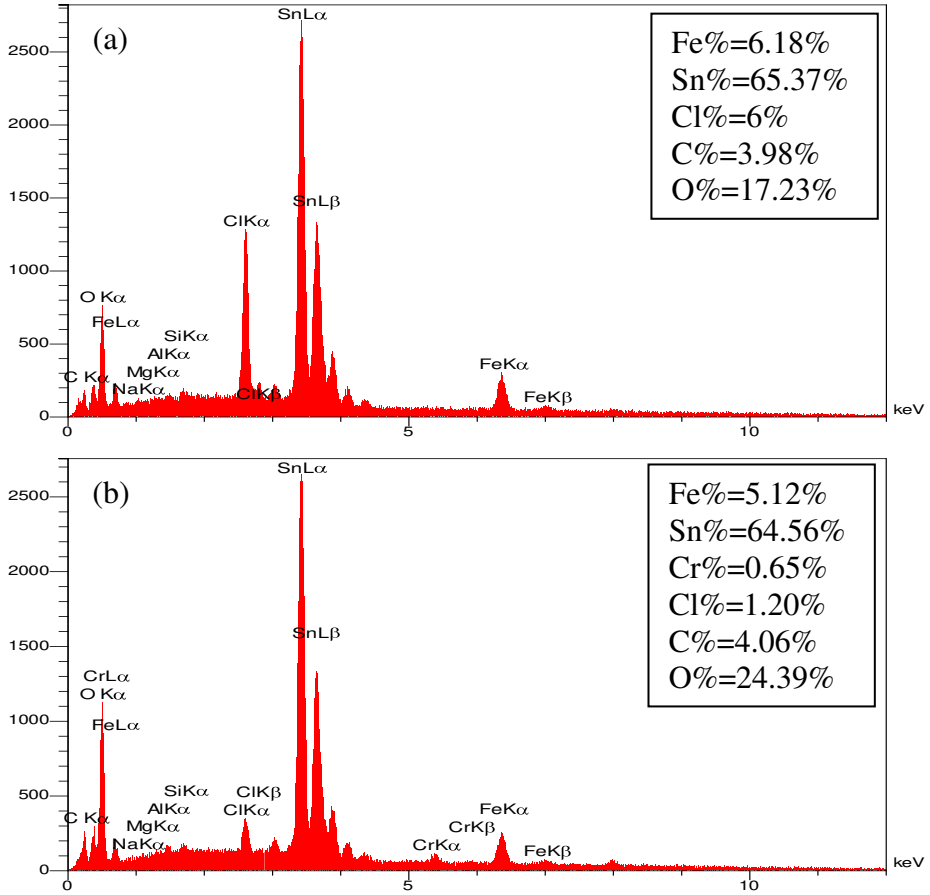

Fig. 3. EDS spectra of (a) Talc-nZVI/6Sn and (b) Talc-nZVI/6Sn after reaction with Cr(VI)

The EDS analysis was applied to clarify the elemental distribution of the different synthesized samples. EDS mapping of the adsorbents with different Sn/Fe loading of 1/1, 4/1, and 6/1 illustrated the uniform distribution of Fe and Sn over the Talc surface (Fig. 2). As can be seen, all samples showed a similar amount of Fe, whereas Sn intensity increased significantly from 17.32 wt% in Talc-nZVI/1Sn to 64.56 wt% in Talc-nZVI/6Sn. Furthermore, the matching distribution of Sn and Fe indicated the coating of Sn on Fe fine particles, which getting thicker as Sn loading increased. Also, EDS mapping of Talc-nZVI/6Sn after Cr(VI) removal process is illustrated in Fig 2(d), which confirmed the presence and distribution of chromium on nZVI/Sn bimetallic particles.

Additionally, the elemental distribution of Talc-nZVI/6Sn before and after Cr(VI) removal was analyzed by EDS (Fig. 3). The EDS results showed that after Cr(VI) removal, despite the nearly constant Fe and Sn loading in both samples, oxygen displayed a meaningful rise from 17.23% to 24.39% along with the appearance of Cr among the elements. The increase in O and Cr content suggested the formation and deposition of Cr(III) hydroxides precipitates on the Talc-nZVI/6Sn surface [32,33].

The BET results reveal the specific surface area and total pore volume in talc equal to 10.84 m^2/g and 0.07 cm^3/g, respectively. The addition of Fe/Sn nanoparticles in Talc-nZVI/6Sn increased the specific surface area and total pore volume to 26.45 m^2/g and 0.1 cm^3/g.

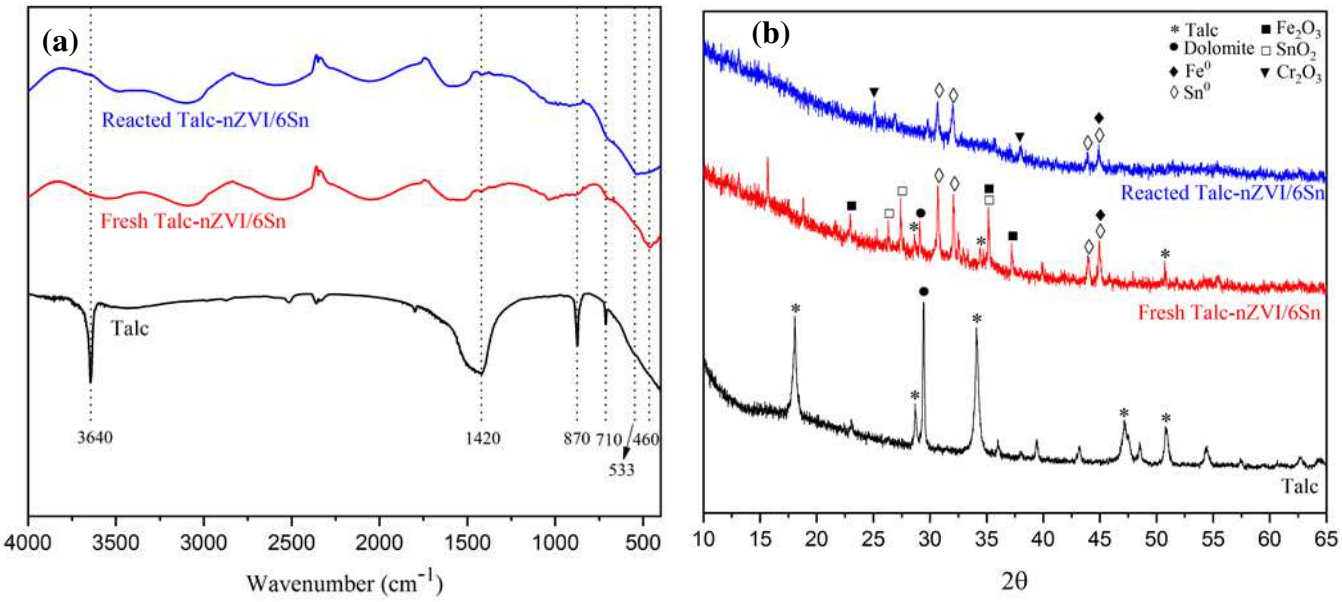

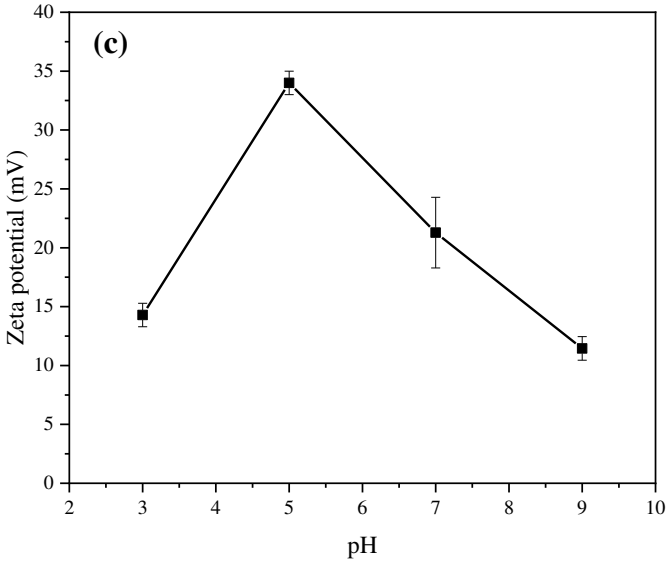

Fig. 4. (a) FTIR spectra and (b) XRD patterns of Talc-nZVI/6Sn before and after Cr(VI) removal, (c) Zeta potential of Talc-nZVI/6Sn at different pH values

The FTIR spectra of talc, Talc-nZVI/6Sn before and after reacting with hexavalent chromium is presented in Fig.4(a). Compared to FTIR spectrum of talc, the fresh synthesized Talc-nZVI/6Sn showed significant changes in peaks including weakening of the bands at 1420 and 3640 cm^{-1} corresponding the −OH group in talc. Also, the bands at 710 and 870 cm^{-1} in talc corresponding Mg−O and Si−O reduced after the impregnation of Fe/Sn bimetallic particles, which is related to the destruction of Mg−O and Si−O bands by alkali, produced during the synthesis of Fe/Sn bimetallic particles through the reaction between $NaBH_4$ and H_2O [34]. Furthermore, the spectrum of fresh Talc-nZVI/6Sn showed a sharp peak at 460 cm^{-1}, which was attributed to Fe−O stretches of Fe_2O_3 and Fe_3O_4, and Sn−O stretches of SnO_2, demonstrating the impregnation of Fe/Sn bimetallic particles on talc surface and partial oxidation of particles surface [35,36]. Despite the similarity in the spectrum of both adsorbents, the reacted Talc-nZVI/6Sn showed changes in the characteristic peaks. The intensity of bands corresponding to the Fe−O and Sn−O stretches at 533 cm^{-1} increased, indicating an

abundance of iron oxides and tin oxides after Cr(VI) removal. Furthermore, the band at 870 cm^{-1} was intensified due to the formation of Cr–O bond, implying the precipitation of Cr on the adsorbent surface [37].

XRD spectra of talc, fresh and reacted Talc-nZVI/6Sn is displayed in Fig. 4(b). XRD pattern of talc, which has been used as supporting material mainly included major peaks at 2θ values of 18°, 28°, 34°, 47°, and 51° for talc and 29.5° for $CaMg(CO_3)_2$/dolomite [32]. The synthesized Talc-nZVI/6Sn XRD pattern composed of the weakened characteristic peaks of talc and quartz and also newly formed peaks of Fe^0 at 2θ of 44.9° and Sn^0 at 2θ of 30°, 32°, 43.9° and 44.9°. The appearance of characteristic peaks of Fe^0 and Sn^0 indicated the successful formation and deposition of Fe/Sn bimetallic nanoparticles on talc surface. Furthermore, some new diffraction peaks emerged, which mainly indicated the formation of a layer of Fe_2O_3 (2θ= 23°, 35°, 37°) and SnO_2 (2θ= 26°, 27°, 35°, 37°) on Fe/Sn bimetallic particles [38]. After Cr(VI) removal, peaks corresponding Fe/Sn bimetallic particles was weakened considerably, indicating that redox reaction happening between Talc-nZVI/6Sn and Cr(VI) leading to the precipitation of the reaction product on adsorbent surface [39]. Additionally, peaks at 2θ of 25° and 37.8° suggested the formation of Cr_2O_3 after Cr(VI) removal. Consistent with the results obtained from EDS and FTIR, these results indicated that Fe/Sn bimetallic nanoparticles has been successfully loaded on talc surface and also, chromium has been appeared on adsorbent surface after Cr(VI) removal reaction.

Also in attempt to get an insight of the adsorbent surface charge, zeta potential of the synthesized adsorbent was investigated at various pH values of 3-9 and illustrated in Fig. 4(c). The results revealed that Talc-nZVI/6Sn have positive surface charge in pH range of 3-9 which is beneficial towards Cr(VI) removal due to the electrostatic attraction between the nanocomposite and chromium negative oxyanions. The results indicated that Talc-nZVI/6Sn is relatively stable in aqueous solution due to its high zeta potential (+34 mV) at pH of 5 [22].

Cr(VI) removal performance of Talc-nZVI/Sn

Effects of Sn/Fe mass ratio

As mentioned previously, Sn coating is used in an attempt to decrease the oxidation of nZVI and also facilitate the electron transfer through formation of many nano-galvanic cells between nZVI and Sn coating. So in order to investigate the extent of enhancement in Cr(VI) removal performance by the effect of Sn/Fe mass loading, a series of composites with varying Sn/Fe mass ratios were prepared, and batch experiments were carried out using 0.15 g (1 g/L) of the composites at constant chromium(VI) concentration of 80 mg/L. As shown in Fig. 5(a), results indicated that increasing Sn mass loading from Sn/Fe mass ratio of 1/1 (Talc-nZVI/Sn) to 8/1 (Talc-nZVI/8Sn) would lead to an increase in removal efficiency from 50% to 85%, respectively.

Talc-nZVI/Sn showed low efficiency in Cr(VI) removal. This was ascribed to the low amount of Sn coating and fast and easy oxidation of nZVI, leading to the formation of a passive layer, which could hinder electron transport between iron nanoparticles and Cr(VI) [40]. The performance of composite enhanced gradually with increasing Sn/Fe mass ratios from 1/1 to 6/1. However, the constant Cr(VI) removal efficiency in Talc-nZVI/6Sn and Talc-nZVI/8Sn indicated the Sn/Fe mass ratio of 6/1 had achieved the full coverage of nZVI particles, and adding an excessive amount of Sn mass loading wouldn't improve the performance of nanocomposite. So Talc-nZVI/6Sn, which provided the Cr(VI) removal efficiency of 85% along with the least Sn loading, was selected as the optimum adsorbent for further experiments.

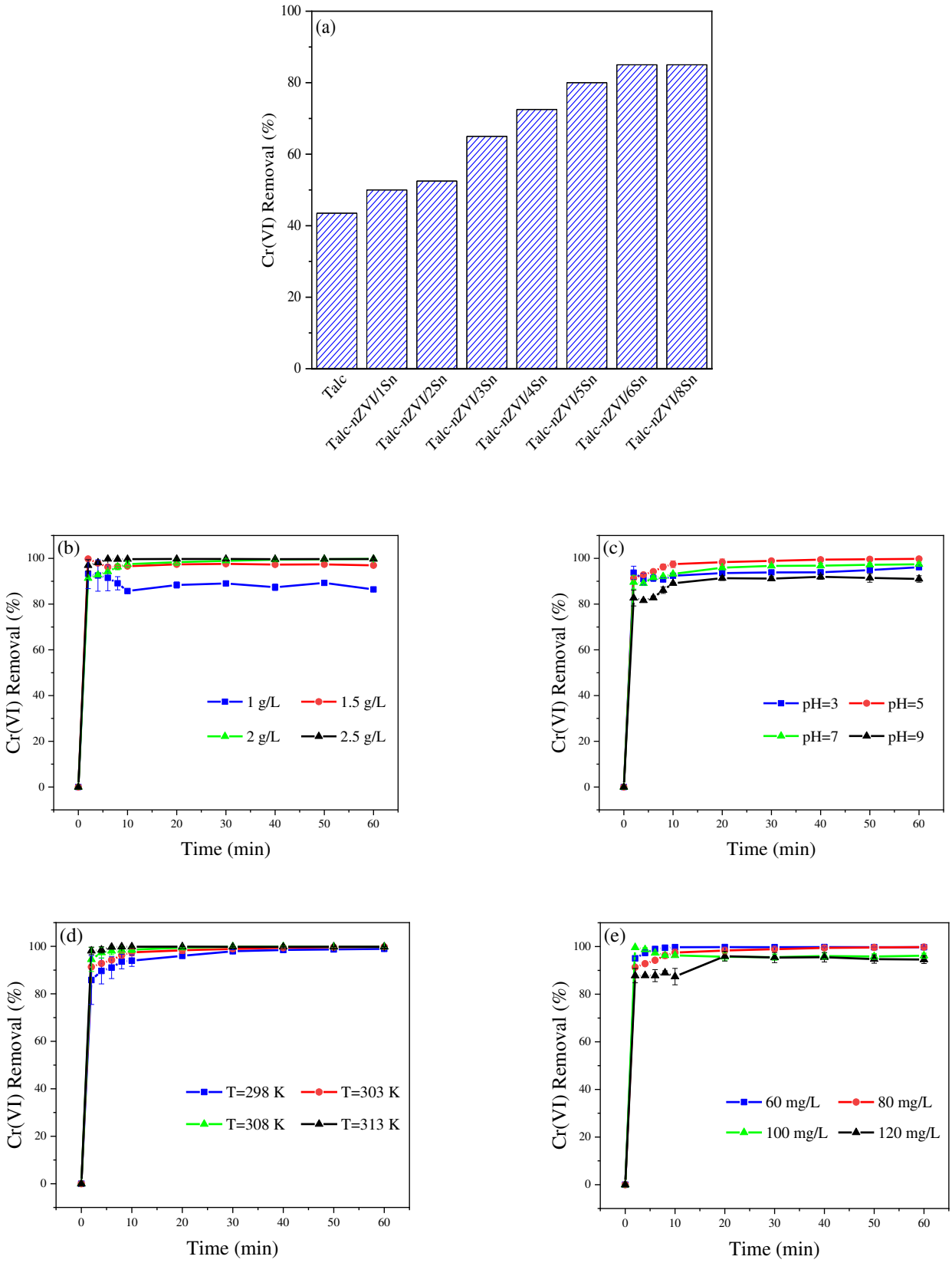

Fig. 5. Effect of (a) Sn/Fe ratio (b) adsorbent dosage (c) pH (d) temperature and (e) initial Cr(VI) concentration on Cr(VI) removal

Effects of Talc-nZVI/Sn dosage

The influence of Talc-nZVI/6Sn dosage on the removal of Cr(VI) from aqueous solution was investigated using various doses (1- 2.5 g/L) at a constant Cr(VI) concentration of 80 mg/L (Fig. 5(b)). With an increase in Talc-nZVI/Sn dosage from 1 to 2.5 g/L, removal efficiency of Cr(VI) increased gradually from 87% to 99.7% after 60 minutes, while removal capacity decreased from 69.6 to 31.9 mg/g, respectively. The reason behind the improvement of removal efficiency is that a higher dosage of composite would provide larger surface area and more available active adsorption sites and more galvanic couples, which could enhance available electrons for Cr(VI) reduction [40]. However, the reduced removal capacity in higher dosage could be due to inter-particle aggregation, overlapping of adsorption sites, and consequently, less active surface area [15,41].

The constant removal efficiency in the dosage of 2 and 2.5 g/L, indicated that Talc-nZVI/6Sn dosage of 2 g/L could offer sufficient active reaction sites for Cr(VI) elimination. Considering efficient performance on Cr(VI) removal of over 99% and low material consumption, a dosage of 2 g/L was selected as the optimum amount of adsorbent.

Effects of pH

The effect of initial pH as an impressive factor on adsorption characteristics was studied within the range of 3-9 at Cr(VI) concentration of 80 mg/L, the temperature of 303 K, and adsorbent amount of 2 g/L. As shown in Fig. 5(c), despite the high Cr(VI) removal at alkaline and neutral conditions, the acidic environment was more conducive for Cr(VI) elimination. It was found that removal efficiency reached its highest value (99.7%) at pH of 5, and reduction ability of Talc-nZVI/6Sn declined with increasing initial pH solution to 7 (97%) and 9 (91%).

Since the initial solution pH strongly affects both surface charge of adsorbent and distribution of Cr(VI), it is among the most important influential factors on Cr(VI) removal efficiency. Solution pH impresses the process in these ways:

(i) In an aqueous solution, Cr(VI) exists in different ionic species which their relative distribution depends on total chromate concentration and the solution pH. In an acidic environment, $HCrO_4^-$ is the dominant species, and in alkaline and neutral conditions, CrO_4^{2-} is the main form of hexavalent chromium [42–44]. $HCrO_4^-$ is more favorable for sorption than CrO_4^{2-} because it has lower adsorption free energy and higher oxidizing capacity (Eqs. (6)-(7)) [40,45]:

$$7H^+ + HCrO_4^- + 3e^- \rightarrow 4H_2O + Cr^{3+} \quad E^0 = 1.35\ (V) \tag{6}$$

$$CrO_4^{2-} + 4H_2O + 3e^- \rightarrow 5OH^- + Cr(OH)_3 \quad E^0 = -0.12\ (V) \tag{7}$$

(ii) The surface charge of the adsorbent is influenced by solution pH. According to the zeta potential measurement in pH range of 3-9 (Fig. 4(c)), adsorbent is positively charged in both acidic and alkaline environments. The electrostatic attraction between the positively charged Talc-nZVI/6Sn and Cr(VI) oxyanions facilitated the contact between adsorbent and contaminant, leading to a better removal performance. Results showed that zeta potential and electrostatic attraction reached to its greatest value at pH of 5, providing Cr(VI) removal efficiency of 99.7%. The positive values of zeta potential and consequently electrostatic attraction between adsorbent and Cr(VI) decreased with the increasing pH, which is consistent with the obtained results in Fig. 5(c).

Furthermore, Table 1 displayed the reduction in solution pH values after the removal process. The decrease in the final solution pH suggested that significant OH^- consumption through the precipitation process has happened.

Table 1. solution pH before and after Cr(VI) removal

Initial pH	3	5	7	9
Final pH	2.97	3.02	3.26	3.37

Effects of temperature

To investigate the effect of temperature on Cr(VI) removal, 2 g/L of Talc-nZVI/6Sn was added to the Cr(VI) aqueous solution with various temperatures of 298, 303, 308, and 313 K. Results shown in Fig. 5(d) revealed that higher temperature conducted to more favorable removal performance which demonstrated that Cr(VI) removal was an endothermic process. With increasing solution temperature from 298 to 303 K, the removal rate of Cr(VI) reached from 98.5% to 99.8%. The further temperature rise, led to the same removal rate of Cr(VI), but in a much shorter time. So that at temperatures of 303 K, the removal efficiency of 99.8% is achieved after 50 minutes of reaction, but the time of reaching the same removal efficiency at temperatures of 308 and 313 K was 30 and 6 minutes, respectively. This can be related to the higher mobility and diffusion rate of Cr(VI) at elevated temperatures of 308 and 313 K, which consequently added to the possibility of contact between chromium ions and the adsorption sites (Lv et al., 2019a; Qiu et al., 2020). Therefore, results suggested that Talc-nZVI/6Sn exhibited substantial performance in removing Cr(VI) under a broad temperature range. Overall, the complete removal of Cr(VI) is obtained at the temperature of 303 K, and more temperature raised only shortened the process time. So the temperature of 303 K is selected as the optimum temperature in the following experiments.

Effects of initial Cr(VI) concentration

Fig. 5(e) revealed the effects of initial Cr(VI) concentration on the performance of Talc-nZVI/6Sn. The results indicated that increasing the initial Cr(VI) concentration from 60 to

120 mg/L, led to lower removal efficiency, whereas provided higher removal capacity. The complete Cr(VI) removal (99.8%) was achieved at initial Cr(VI) concentration of 60 and 80 mg/L, but with increasing initial Cr(VI) concentration to 100 and 120 mg/L, Cr(VI) removal declined to 96% and 95%, respectively. Obviously, a constant amount of Talc-nZVI/6Sn provided a definite amount of adsorption active sites, which finally would be occupied by increasing Cr(VI) concentration. Furthermore, higher Cr(VI) concentration conducted to more precipitation of removal products on the adsorbent surface, hindering the electron transfer between talc-nZVI/6Sn and Cr species. Overall, both terms contributed to decreased removal efficiency in higher Cr(VI) concentrations. However, the removal capacity of 56 mg/g at Cr(VI) concentration of 120 mg/L, exhibited the great ability of Talc-nZVI/6Sn for Cr(VI) elimination (Fu et al., 2015b; Lv et al., 2019b).

Galvanic performance of Fe/Sn bimetallic nanoparticles

To elucidate the galvanic performance of nZVI/Sn nanoparticles, four different metallic cations were added to the aqueous solution of Cr(VI), and their effects on Cr(VI) removal was illustrated for Talc-nZVI/3Sn (Fig. 6(a)) and Talc-nZVI/6Sn (Fig. 6(b)). Despite the expectation that the co-existing metallic cations would compete with C(VI) anions for the limited amount of galvanic cells, results demonstrated that adding metallic cations mostly increased the Cr(VI) removal efficiency, indicating their synergistic role in facilitating electron transfer to chromium oxyanions. By using Talc-nZVI/3Sn, presence of metallic cations increased the Cr(VI) removal efficiency in order of Cu(II)>Hg(II)>Co(II)>Cd(II). In case of using Talc-nZVI/6Sn, the presence of Cu(II) and Hg(II) caused the Cr(VI) removal efficiency to increase from 86% to 96% and 89%, respectively. The improved performance of both nanocomposites in Cr(VI) removal could be ascribed to the adsorption and deposition of the added cationic metals to the nZVI/Sn bimetallic particles and the formation of trimetallic

nZVI/Sn/M particles (M: Hg(II), Cu(II), Co(II), Cd(II)), which could facilitate and enhance the electron transfer to Cr(VI) [29]. The maximum enhanced catalytic performance of the metallic cations was related to the presence of Cu(II) which caused 14% and 10% increase in Cr(VI) removal efficiency of Talc-nZVI/3Sn and Talc-nZVI/6Sn, respectively. The higher improvement in Cr(VI) removal capacity of Talc-nZVI/3Sn compared to the Talc-nZVI/6Sn could be attributed to the less coverage of nZVI particles in Talc-nZVI/3Sn which provided more nZVI cores for the deposition of metallic cations. In addition, results indicated that the presence of Co(II) and Cd(II) lead to decline in Cr(VI) elimination in case of using Talc-nZVI/6Sn. This decrease was related to the lower standard reduction potentials of Co(II) ($E^0(Co^{2+}/Co) = -0.28\,V$) and Cd(II) ($E^0(Cd^{2+}/Cd) = -0.4\,V$) compared to the Sn shell layer ($E^0(Sn^{2+}/Sn) = -0.13\,V$) which consequently would eliminate the electron flow of the nZVI/Sn nano-galvanic cells.

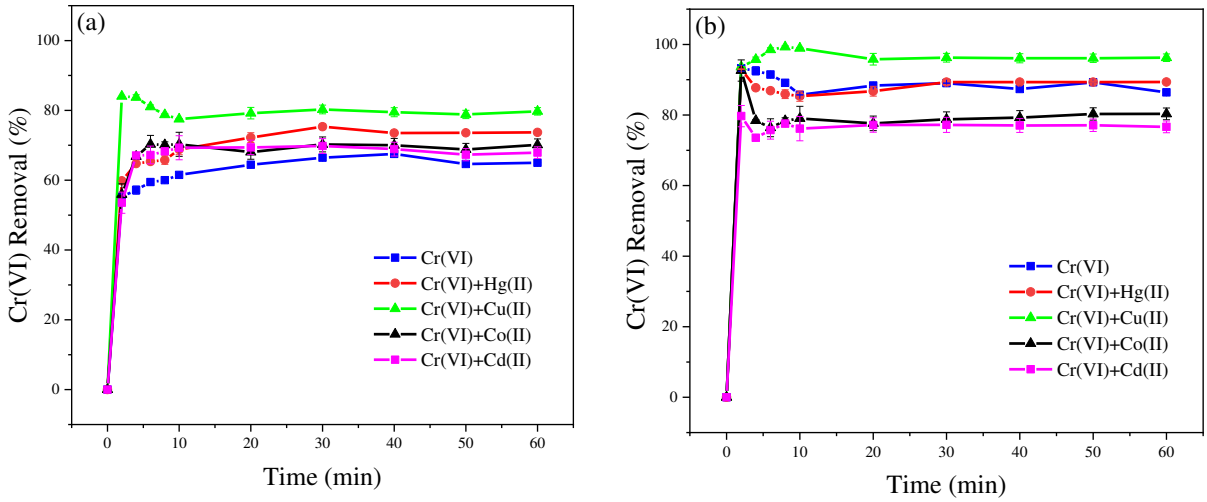

Fig. 6. The effects of metallic cation's presence on the Cr(VI) removal using (a) Talc-nZVI/3Sn and (b) Talc-nZVI/6Sn (Cr(VI) initial concentration: 80 mg/L, metallic cations initial concentration: 40 mg/L, nanocomposite dosage: 1 g/L)

Aging study and reusability of Talc-nZVI/Sn

Regarding the protective role of Sn coating on nZVI particles, an aging study of Talc-nZVI/6Sn was carried out every 10 days to reveal the effect of time on nZVI activity (Fig. 7(a)). As shown in Fig. 7(a), Talc-nZVI/6Sn was found to keep its high removal capacity for nearly two months, which provide considerably better stability compared to previous studies (Lv et al., 2019a; Zhou et al., 2016). The significant stability of Talc-nZVI/6Sn could be attributed to the full coverage of Sn coating on nZVI particles, providing an inhibitive layer to nZVI oxidation.

Furthermore, Talc-nZVI/6Sn was repeatedly used and regenerated to investigate its reusability (Fig. 7(b)). Results indicated that after the first regeneration, the bimetallic nanocomposite displayed a remarkable decline in removal efficiency (68%). Additionally, the second regeneration led to Cr(VI) removal efficiency of less than 50%. The low removal efficiency in Cr(VI) removal could be related to the deposition of precipitates on nanocomposites, eliminating the regeneration process.

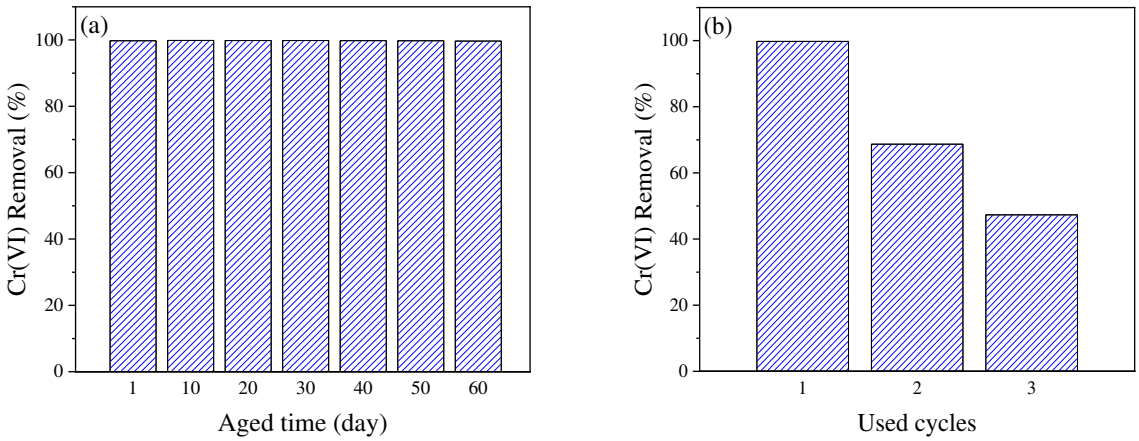

Fig. 7. (a) Aging study and (b) reusability of Talc-nZVI/6Sn

Adsorption kinetics

Adsorption kinetic study provides an estimation of adsorption rates along with possible reaction mechanisms [42]. Regarding the rate of solute adsorption and reactant concentration, various kinetic models can be applied to describe the rate of the adsorption process. Here, three kinetic models were used, including the pseudo-first-order (Eq. (8)), pseudo-second-order (Eq. (9)), and intraparticle diffusion (Eq. (10)) models, represented as follows [15]:

$$\ln(q_e - q_t) = \ln(q_e) - k_1 t \quad (8)$$

$$t/q_t = 1/k_2 q_e^2 + t/q_e \quad (9)$$

$$q_t = k_i t^{0.5} + C \quad (10)$$

where q_e and q_t (mg/g) represent the adsorption capacities at equilibrium and at time t (min), respectively; k_1 and k_2 are the rate constants for the pseudo-first-order and pseudo-second-order; k_i is the rate constant for the intraparticle diffusion and C is the intercept.

The Cr(VI) elimination kinetics was studied using 2 g/L talc-nZVI/6Sn at different Cr(VI) initial concentrations of 60, 80, 100, and 120 mg/L and the calculated model parameters were displayed in Table 2. As result shown, the Cr(VI) removal process was in accordance with the pseudo-second-order model (R^2>0.999) compared to the other models. Also, the calculated Cr(VI) removal capacity was consistent with the experimental results. With increasing Cr(VI) concentration from 60 to 120 mg/L, the pseudo-second-order rate constant k_2 decreased in general from 0.317 to 0.080 (g/mg min). The results revealed that chemisorption was the rate-limiting step in Cr(VI) removal, and chemisorptive bonds, including sharing or exchanging electrons between Cr(VI) and Talc-nZVI/6Sn were involved [32,48]. The result is consistent with the FTIR and XRD findings.

Table 2. Kinetic parameters for Cr(VI) removal by Talc-nZVI/6Sn

Kinetic model	Initial Cr(VI) concentration (mg/L)	Parameters		
Pseudo-first		q_e (mg/g)	k_1 (1/min)	R^2

order	60	29.826	1.545	0.9995
	80	39.024	1.324	0.9940
	100	48.123	3.955	0.9976
	120	55.261	1.485	0.9849
		q_e (mg/g)	k_2 (g/mg min)	R^2
Pseudo-second order	60	30.078	0.317	0.9998
	80	39.760	0.117	0.9988
	100	48.565	0.519	0.9999
	120	56.470	0.080	0.9905
		C	k_i (mg/(g $min^{0.5}$))	R^2
Intraparticle diffusion	60	19.336	1.959	0.2199
	80	24.336	2.784	0.2789
	100	24.161	4.387	0.3385
	120	33.998	4.090	0.3035

Adsorption isotherm analysis

In an attempt to better understand the adsorption of Cr(VI) by Talc-nZVI/6Sn, four isotherm models were applied to fit the experimental data, and the results were summarized in Table 3. Adsorption isotherm models including Langmuir (Eq. (11)), Freundlich (Eq. (12)), Sips (Eq. (13)), and Temkin (Eq. (14)) were used:

$$q_e = \frac{q_m K_L C_e}{1+K_L C_e} \quad (11)$$

$$q_e = K_F C_e^{1/n_F} \quad (12)$$

$$q_e = \frac{q_m (K_S C_e)^{n_S}}{1+(K_S C_e)^{n_S}} \quad (13)$$

$$q_e = \frac{RT}{b} \ln K_T + \frac{RT}{b} \ln C_e \quad (14)$$

where q_e is the adsorption capacity at equilibrium (mg/g), q_m is the maximum adsorption capacity, C_e is the equilibrium concentration of Cr(VI) (mg/L). K_L (L/mg) and K_F (mg^{1-}

$^{1/nF}$.L$^{1/nF}$/g) are the Langmuir and Freundlich constants, respectively and $1/n_F$ is the heterogeneity factor. In Sips model, which is a combination of Langmuir and Freundlich isotherm models, K_S is the Sips constant, and n_s is the Sips isotherm exponent. Also, in the Temkin equation, b is the Temkin constant related to the heat of adsorption (J/mol), R is the universal gas constant (J/mol K), T is the temperature (K), and K_T is the Temkin isotherm constant (L/g).

Results showed that the Langmuir isotherm model yielded the best fitting results (R^2 = 0.97958) compared to other models (Table 3). The results are in agreement with previous studies on Cr(VI) removal using similar adsorbents. According to the Langmuir model, adsorption of Cr(V) on the Talc-nZVI/6Sn occurred through monolayer adsorption, and all active sites were homogeneous and energetically equivalent. Furthermore, the Langmuir isotherm model assumes that each site can bind a single adsorbate molecule, and there is no interaction between two adsorbed pollutant molecules. Also, the Langmuir model indicates that adsorption processes are controlled by chemical reactions [16,49].

Table 3. Adsorption isotherm model parameters for Cr(VI) removal by Talc-nZVI/Sn

Isotherm model	Parameters			R^2
Langmuir	q_m (mg/g)	K_L (L/mg)		
	53.5244	13.35524		0.97958
Freundlich	K_F (mg$^{1-1/n}$.L$^{1/n}$/g)	1/n		
	43.67506	0.121405		0.97581
Sips	q_m (mg/g)	K_S (L/mg)	n_s	
	43.4401	24.95368	1.05354	0.97309
Temkin	K_T (L/g)	b (J/mol)		

	5036.517	480.5157	0.97692

Cr(VI) Removal Mechanism

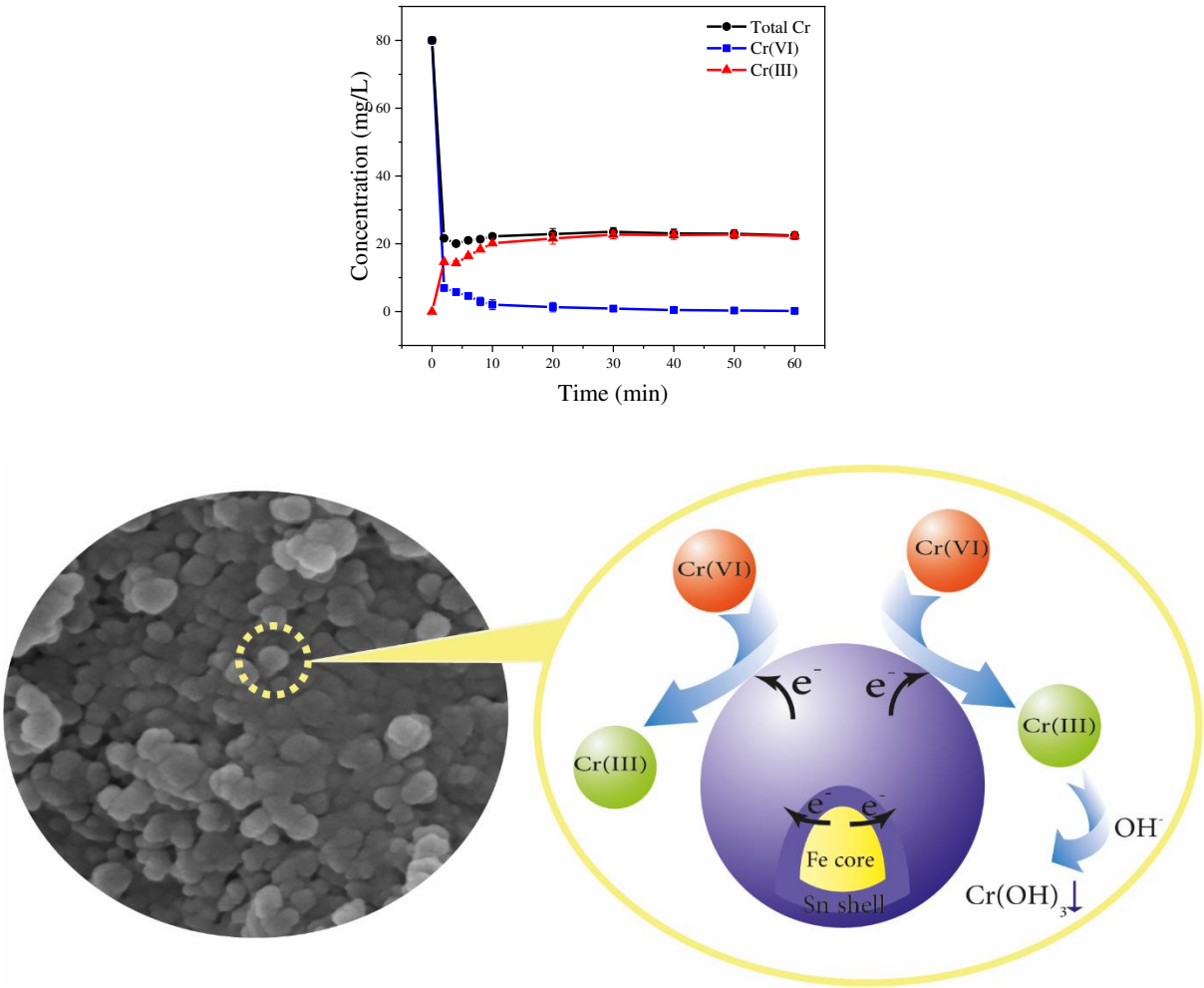

Fig. 8. (a) The variation of Cr concentration in aqueous solution (initial Cr(VI) concentration: 80 mg/L, temperature: 30 ℃, pH: 5, adsorbent dosage: 2 g/L) (b) Proposed mechanism of Cr(VI) removal by Talc-nZVI/6Sn

The changes in Cr concentration (total Cr, Cr(VI), and Cr(III)) in aqueous solution during reaction time using Talc-nZVI/6Sn was illustrated in Fig. 8(a). Total Cr concentration showed a sharp decrease after 4 minutes of the reaction, and reached to the constant value of 22 mg/L, suggesting that 58 mg/L of chromium is combined with Talc-nZVI/6Sn in forms of

Cr(VI) and/or Cr(III). Hexavalent chromium followed a similar trend to total chromium, but reached to a much less value of 0.1 mg/L after 60 minutes, which could be ascribed to both the adsorption on Talc-nZVI/6Sn surface and reduction to Cr(III). Meanwhile, Cr(III) increased gradually and became the dominant form of chromium in the solution.

According to the mentioned discussions, Cr(VI) removal by Talc-nZVI/6Sn consisted of multiple processes of adsorption-reduction and precipitation process, reinforced by the numerous nano-galvanic cells of nZVI/Sn bimetallic particles (Fig. 8(b)). nZVI/Sn bimetallic particles formed galvanic cells wherein iron and tin acted as anode and cathode, respectively. The galvanic cell effects catalytically enhanced the electron transfer to Cr(VI). Simultaneously, the transferred electron reduced Cr(VI) to Cr(III) (Fu et al., 2015a). Based on the XRD and FTIR analysis of the reacted adsorbent, and the final solution pH (Table 1), the Cr(III) precipitation happened ultimately. The possible reactions are expressed by Eqs. (15)- (18) as follows:

$$3Fe^0 - Sn^0 + 2HCrO_4^- + 14H^+ \rightarrow 3Fe^0 - Sn^{2+} + 2Cr^{3+} + 8H_2O \quad (15)$$

$$3Fe^0 - Sn^0 + Cr_2O_7^{2-} + 14H^+ \rightarrow 3Fe^0 - Sn^{2+} + 2Cr^{3+} + 7H_2O \quad (16)$$

$$3Fe^0 - Sn^0 + 2CrO_4^{2-} + 16H^+ \rightarrow 3Fe^0 - Sn^{2+} + 2Cr^{3+} + 8H_2O \quad (17)$$

$$2Cr^{3+} + 6OH^- \leftrightarrow 2Cr(OH)_3(s) \leftrightarrow Cr_2O_3(s) + 3H_2O \quad (18)$$

Comparison of Cr(VI) removal by similar nZVI-based materials

A comparison between the removal capacity of Talc-nZVI/6Sn and some similar previous researches using supported-nZVI particles is presented at Table 4. It could be found that Talc-nZVI/6Sn provided higher and in some cases similar Cr(VI) removal potentials. The high removal capacity (56 mg/g), great longevity, simplicity of synthesis method, and affordable raw materials used as support and coating of nZVI particles, demonstrated the high capability of Talc-nZVI/6Sn in remediation of Cr-contaminated resources.

Table 4. Comparison of maximum removal capacity of Cr(VI) by supported-nZVI materials

Materials	Material dosage (g/L)	pH	Removal capacity (mg/g)	source
Bentonite-supported nZVI	10	6	7.3	[51]
Sepiolite-supported nZVI	1.6	6	43.86	[7]
Amino-functionalized vermiculite-supported nZVI	0.625	5	59.17	[22]
Montmorillonite-supported nZVI	0.22	5.5	31.65	[52]
Kaolin-supported nZVI	2	4	33.39	[53]
Bentonite-supported organosolv lignin-stabilized nZVI	1	3	50	[54]
Graphene nanosheets-supported nZVI	1	7	21.72	[5]
Biochar-supported nZVI	1.5	4	35.30	[55]
Biochar-supported nZVI	-	4	40	[56]
Talc-supported nZVI/Sn	2	5	56	This study

Conclusions

Talc supported nano-galvanic nZVI/Sn bimetallic particles were prepared and utilized for hexavalent chromium elimination. Nanocomposites with varying Sn/Fe mass ratio from 1/1 to 8/1 was synthesized and optimized for Cr(VI) removal reaction. SEM analysis, mapping, and EDS spectra of the materials indicated the core-shell bimetallic nZVI/Sn particles were

deposited on talc layered structure while the shell thickness increase with rising Sn/Fe mass ratio. Furthermore, other influential factors, including nanocomposite dosage, pH, temperature, and initial Cr(VI) concentration were investigated. The highest Cr(VI) removal efficiency of 99.8% was achieved using Sn/Fe mass ratio of 6/1, the adsorbent dosage of 2 g/L, pH of 5, the temperature of 303 K, and initial Cr(VI) concentration of 80 mg/L after 10 minutes of reaction. Monitoring the co-existing of metallic cations on the galvanic performance of Talc-nZVI/3Sn and Talc-nZVI/6Sn revealed the synergistic effects of cations through formation of trimetallic particles which lead to 14% and 10% increase in Cr(VI) removal efficiency, respectively. Talc-nZVI/6Sn preserved the high capacity for Cr(VI) elimination for 60 days due to the thick and protective layer of Sn on nZVI active sites. However, the ability of nanocomposite for regeneration was limited, and its efficiency declined to less than 50% after 2 times of regeneration. The reaction results were in accordance with the pseudo-second-order kinetic model and the Langmuir isotherm model in which Cr(VI) removal was controlled by chemical reactions. Finally, the Cr(VI) removal process was speculated to follow adsorption, reduction, and precipitation of products, which was enhanced by the galvanic cell effects of nZVI/Sn bimetallic particles.

Materials and methods

Chemicals

A commercial Iranian talc with a mesh size of 325 was used. All chemicals including ferric chloride hexahydrate ($FeCl_3.6H_2O$), tin(II) Chloride dihydrate ($SnCl_2.2H_2O$), potassium dichromate ($K_2Cr_2O_7$), sodium borohydride ($NaBH_4$), diphenylcarbazide ($C_{13}H_{14}N_4O$), ethanol (99.7%), sodium hydroxide ($NaOH$), hydrochloric acid (HCl), sulfuric acid (H_2SO_4) and metallic cations ($HgCl_2$, $CuCl_2.2H_2O$, $CoCl_2.6H_2O$, $CdCl_2.H_2O$) were of analytical grade

and were purchased from Merck. All the chemicals were used as received from the supplier without further purification.

Preparation of nZVI and Talc-nZVI/Sn nanoparticles

Chemical reduction, as the most frequent synthesis technique of nZVI has been utilized to prepare the bimetallic particles, due to its simplicity and homogeneous structure of the products [20]. Based on their synthesis method, bimetallic nanoparticles would have different structures such as alloy, core-shell, and contact aggregate [26]. Since this study aimed to achieve a core-shell structure deposited on talc, a two-step reduction method was employed.

At first, talc was washed, filtered, and dried at 90 ℃ overnight prior to the experiment. $FeCl_3.6H_2O$ and talc (mass ratio of talc:Fe^{3+} at 2:1) were dissolved in 100 mL solution of ethanol and deionized water (70%, v/v) and mixed for 30 minutes and 200 rpm in a three-neck flask. Then the freshly prepared reducing agent ($NaBH_4$, 50 mL, 1.07 M) was added dropwise (1-2 drops in every second) into the solution along with vigorous stirring. Immediately with the addition of the first drop of the sodium borohydride, the color of the solution turned black. After adding all of $NaBH_4$ solution, mixing continued for another 30 minutes to ensure the maximum yield in nZVI production and deposition on talc. Theoretically, the reaction in the process occurred in three following steps [Eqs. (1) to (3)] [21]:

$$4Fe^{3+} + BH_4^- + 3H_2O \rightarrow 4Fe^{2+} + H_2BO_3^- + 4H^+ + 2H_2 \uparrow \quad (1)$$

$$2Fe^{2+} + BH_4^- + 3H_2O \rightarrow 2Fe^0 \downarrow + H_2BO_3^- + 4H^+ + 2H_2 \uparrow \quad (2)$$

$$4Fe^{3+} + 3BH_4^- + 9H_2O \rightarrow 4Fe^0 \downarrow + 3H_2BO_3^- + 12H^+ + 6H_2 \uparrow \quad (3)$$

Afterward, $SnCl_2.2H_2O$ was added to the mixture with different Sn/Fe mass ratios (1/1, 2/1, 3/1, 4/1, 6/1, 8/1) and under continuous stirring for 30 minutes. Finally, the prepared nanoparticles were separated using vacuum filtration, washed three times with ethanol, and

dried for 12 h at 60 ℃. The whole process was performed under continuous nitrogen gas purging.

Batch experiments

The batch experiments were conducted in duplicates in a glass beaker containing 150 mL of Cr(VI) solution. Basically, the synthesized nanocomposite was added to the beaker that contained Cr(VI) solution at 303 K and pH of 5, under continuous stirring (300 rpm) for 60 minutes. At specific time intervals, the supernatant was taken out and immediately filtered to separate the particles through a 0.45 mm filter membrane. Afterward, dilution and acidification of the sample were carried out to measure the residual concentrations of Cr(VI). The effects of Sn/Fe mass ratio (1/1, 2/1, 3/1, 4/1, 6/1, 8/1), Talc-nZVI/Sn dosage (1- 2.5 g/L), pH (3- 9), temperature (298- 313 K) and Cr(VI) initial concentration (60- 120 mg/L) on the removal performance were studied.

A stock solution of Cr(VI) (1000 mg/L) was prepared and diluted with deionized water to achieve the desired concentration of Cr(VI) solution. The initial pH values of the Cr(VI) solution was adjusted using 0.1 M HCl or 0.1 M NaOH.

The removal efficiency and the removal capacity of Cr(VI) at equilibrium was determined by the following equations (4) and (5):

$$R = \frac{C_0 - C_t}{C_0} \times 100\% \quad (4)$$

$$q_t = \frac{(C_0 - C_t) \times V}{m} \quad (5)$$

Where R is the removal efficiency of Cr(VI), and C_0 and C_t (mg/L) are the initial and equilibrium concentrations of Cr(VI), respectively. Also, q_t (mg/g) represents the removal capacity of hexavalent chromium at a contact time of t (min). Finally, V (L) is the volume of Cr(VI) solution tested, and m (g) represents the weight of Talc-nZVI/Sn added to the solution.

In addition, the effects of co-existing metallic cations with different reduction potentials on the performance of nanocomposite in Cr(VI) was investigated. In these experiments, metallic cations including Hg(II), Cu(II), Co(II) and Cd(II) with initial concentration of 40 mg/L and Cr(VI) with initial concentration of 80 mg/L was tested using nanocomposite amount of 1 g/L at pH: 5 and T: 30 ℃.

Also, the reusability of the synthesized adsorbent was investigated through sequential Cr(VI) remediation and adsorbent regeneration. In this regard, after Cr(VI) removal reaction, Talc-nZVI/Sn was collected and chemically reduced using $NaBH_4$ solution (50 mL, 1.07 M) stirring for 60 min. Afterwards, the regenerated adsorbent is washed with ethanol for three times, dried for 12 h at 60 ℃, and used for Cr(VI) remediation. Finally, the effect of aging on the activity of the synthesized Talc-nZVI/Sn was investigated for 60 days (every 10 days). All of the experiments were conducted in duplicate.

Characterization and analysis methods

The surface morphology and elemental distribution of the different synthesized nanocomposites were obtained using field emission scanning electron microscopy (SEM, MIRA3 TESCAN, USA) equipped with energy dispersive spectroscopy (SEM-EDS) system. The crystal structure of the fresh and reacted nanocomposites were analyzed by X-ray diffraction (XRD, X-Ray Explorer, GNR, Italy) using Cu-Kα radiation. An infrared spectrometer was used to obtain the Fourier transform infrared spectroscopy (FTIR) spectra of Talc-nZVI/6Sn before and after Cr(VI) removal reaction (Nicolet iS10, Thermo Scientific, USA). Zeta potentials were measured at various pH values by Wallis zeta potential analyzer (Cordouan Technologies, France) at 25 ℃.

Brunauer–Emmett–Teller (BET) N_2 adsorption analysis was performed to obtain the specific surface area of the particles using a surface area analyzer (Autosorb-1-MP, Quantachrome

Instruments, USA). The Cr(VI) concentration was detected by the 1,5-diphenylcarbazide method with a UV-vis spectrophotometer at a wavelength of 540 nm. Total Cr concentration was determined using flame atomic absorbance spectrometer and the Cr(III) concentration was calculated by subtracting Cr(VI) from total Cr concentration.

References

1. Wu, Y. *et al.* Environmental remediation of heavy metal ions by novel-nanomaterials: A review. *Environ. Pollut.* **246**, 608–620 (2019).
2. Zou, Y. *et al.* Environmental Remediation and Application of Nanoscale Zero-Valent Iron and Its Composites for the Removal of Heavy Metal Ions: A Review. *Environ. Sci. Technol.* **50**, 7290–7304 (2016).
3. Fu, F. & Wang, Q. Removal of heavy metal ions from wastewaters: A review. *J. Environ. Manage.* **92**, 407–418 (2011).
4. O'Carroll, D., Sleep, B., Krol, M., Boparai, H. & Kocur, C. Nanoscale zero valent iron and bimetallic particles for contaminated site remediation. *Adv. Water Resour.* **51**, 104–122 (2013).
5. Li, X., Ai, L. & Jiang, J. Nanoscale zerovalent iron decorated on graphene nanosheets for Cr(VI) removal from aqueous solution: Surface corrosion retard induced the enhanced performance. *Chem. Eng. J.* **288**, 789–797 (2016).
6. Vilardi, G., Ochando-Pulido, J. M., Verdone, N., Stoller, M. & Di Palma, L. On the removal of hexavalent chromium by olive stones coated by iron-based nanoparticles: Equilibrium study and chromium recovery. *J. Clean. Prod.* **190**, 200–210 (2018).
7. Fu, R. *et al.* The removal of chromium (VI) and lead (II) from groundwater using sepiolite-supported nanoscale zero-valent iron (S-NZVI). *Chemosphere* **138**, 726–734 (2015).
8. Zhu, F., Li, L., Ma, S. & Shang, Z. Effect factors, kinetics and thermodynamics of remediation in the chromium contaminated soils by nanoscale zero valent Fe/Cu bimetallic particles. *Chem. Eng. J.* **302**, 663–669 (2016).
9. Kadu, B. S. & Chikate, R. C. NZVI based nanocomposites: Role of noble metal and clay support on chemisorptive removal of Cr(VI). *J. Environ. Chem. Eng.* **1**, 320–327

(2013).

10. Jiang, D. *et al.* Difunctional chitosan-stabilized Fe/Cu bimetallic nanoparticles for removal of hexavalent chromium wastewater. *Sci. Total Environ.* **644**, 1181–1189 (2018).

11. Vardhan, K. H., Kumar, P. S. & Panda, R. C. A review on heavy metal pollution, toxicity and remedial measures: Current trends and future perspectives. *J. Mol. Liq.* **290**, 111197 (2019).

12. Joseph, L., Jun, B. M., Flora, J. R. V., Park, C. M. & Yoon, Y. Removal of heavy metals from water sources in the developing world using low-cost materials: A review. *Chemosphere* **229**, 142–159 (2019).

13. Bolisetty, S., Peydayesh, M. & Mezzenga, R. Sustainable technologies for water purification from heavy metals: review and analysis. *Chem. Soc. Rev.* **48**, 463–487 (2019).

14. Yadav, V. B., Gadi, R. & Kalra, S. Clay based nanocomposites for removal of heavy metals from water: A review. *J. Environ. Manage.* **232**, 803–817 (2019).

15. Wadhawan, S., Jain, A., Nayyar, J. & Mehta, S. K. Role of nanomaterials as adsorbents in heavy metal ion removal from waste water: A review. *J. Water Process Eng.* **33**, (2020).

16. Yang, J. *et al.* Nanomaterials for the Removal of Heavy Metals from Wastewater. *Nanomaterials* **9**, 424 (2019).

17. Burakov, A. E. *et al.* Adsorption of heavy metals on conventional and nanostructured materials for wastewater treatment purposes: A review. *Ecotoxicol. Environ. Saf.* **148**, 702–712 (2018).

18. Renu, Agarwal, M. & Singh, K. Heavy metal removal from wastewater using various adsorbents: A review. *J. Water Reuse Desalin.* **7**, 387–419 (2017).

19. Wu, L., Liao, L., Lv, G. & Qin, F. Stability and pH-independence of nano-zero-valent iron intercalated montmorillonite and its application on Cr(VI) removal. *J. Contam. Hydrol.* **179**, 1–9 (2015).

20. Stefaniuk, M., Oleszczuk, P. & Ok, Y. S. Review on nano zerovalent iron (nZVI): From synthesis to environmental applications. *Chem. Eng. J.* **287**, 618–632 (2016).

21. Ezzatahmadi, N. *et al.* Clay-supported nanoscale zero-valent iron composite materials for the remediation of contaminated aqueous solutions: A review. *Chem. Eng. J.* **312**, 336–350 (2017).

22. Zhao, R., Zhou, Z., Zhao, X. & Jing, G. Enhanced Cr(VI) removal from simulated electroplating rinse wastewater by amino-functionalized vermiculite-supported nanoscale zero-valent iron. *Chemosphere* **218**, 458–467 (2019).

23. Wang, J., Liu, G., Zhou, C., Li, T. & Liu, J. Synthesis, characterization and aging study of kaolinite-supported zero-valent iron nanoparticles and its application for Ni(II) adsorption. *Mater. Res. Bull.* **60**, 421–432 (2014).

24. He, Y., Sun, H., Liu, W., Yang, W. & Lin, A. Study on removal effect of Cr(VI) and surface reaction mechanisms by bimetallic system in aqueous solution. *Environ. Technol.* **0**, 1–23 (2018).

25. Wu, Y., Yue, Q., Gao, Y., Ren, Z. & Gao, B. Performance of bimetallic nanoscale zero-valent iron particles for removal of oxytetracycline. *J. Environ. Sci. (China)* **69**, 173–182 (2018).

26. Sharma, G. *et al.* Novel development of nanoparticles to bimetallic nanoparticles and their composites: A review. *J. King Saud Univ. - Sci.* **31**, 257–269 (2019).

27. Shi, L., Du, J., Chen, Z., Megharaj, M. & Naidu, R. Functional kaolinite supported Fe/Ni nanoparticles for simultaneous catalytic remediation of mixed contaminants (lead and nitrate) from wastewater. *J. Colloid Interface Sci.* **428**, 302–307 (2014).

28. Kadu, B. S. *et al.* Efficiency and recycling capability of montmorillonite supported Fe-Ni bimetallic nanocomposites towards hexavalent chromium remediation. *Appl. Catal. B Environ.* **104**, 407–414 (2011).

29. Cai, X. *et al.* Removal of co-contaminants Cu (II) and nitrate from aqueous solution using kaolin-Fe/Ni nanoparticles. *Chem. Eng. J.* **244**, 19–26 (2014).

30. Shameli, K., Ahmad, M. Bin, Al-Mulla, E. A. J., Shabanzadeh, P. & Bagheri, S. Antibacterial effect of silver nanoparticles on talc composites. *Res. Chem. Intermed.* **41**, 251–263 (2013).

31. Kalantari, K. *et al.* Rapid adsorption of heavy metals by Fe3O4/talc nanocomposite and optimization study using response surface methodology. *Int. J. Mol. Sci.* **15**, 12913–12927 (2014).

32. Zhang, Y., Jiao, X., Liu, N., Lv, J. & Yang, Y. Enhanced removal of aqueous Cr(VI) by a green synthesized nanoscale zero-valent iron supported on oak wood biochar. *Chemosphere* **245**, (2020).

33. Zhou, X., Jing, G., Lv, B., Zhou, Z. & Zhu, R. Highly efficient removal of chromium(VI) by Fe/Ni bimetallic nanoparticles in an ultrasound-assisted system. *Chemosphere* **160**, 332–341 (2016).

34. Zhang, X., Lin, S., Chen, Z., Megharaj, M. & Naidu, R. Kaolinite-supported nanoscale zero-valent iron for removal of Pb2+ from aqueous solution: Reactivity, characterization and mechanism. *Water Res.* **45**, 3481–3488 (2011).

35. Zhu, F., Ma, S., Liu, T. & Deng, X. Green synthesis of nano zero-valent iron/Cu by green tea to remove hexavalent chromium from groundwater. *J. Clean. Prod.* **174**, 184–190 (2018).

36. Feng, Y. S., Zhou, S. M., Li, Y., Li, C. C. & Zhang, L. D. Synthesis and characterization of tin oxide nanoparticles dispersed in monolithic mesoporous silica.

Solid State Sci. **5**, 729–733 (2003).

37. Xiang, K., Pandey, R., Recio, J. M., Francisco, E. & Newsam, J. M. A Theoretical Study of the Cluster Vibrations in Cr 2 O 2 , Cr 2 O 3 , and Cr 2 O 4. *J. Phys. Chem. A* **104**, 990–994 (2000).

38. Hadia, N. M. A., Ryabtsev, S. V., Seredin, P. V. & Domashevskaya, E. P. Effect of the temperatures on structural and optical properties of tin oxide (SnOx) powder. *Phys. B Condens. Matter* **405**, 313–317 (2010).

39. Zhang, W. *et al.* Effective removal of Cr(VI) by attapulgite-supported nanoscale zero-valent iron from aqueous solution: Enhanced adsorption and crystallization. *Chemosphere* **221**, 683–692 (2019).

40. Wu, J. *et al.* Preparation of highly dispersive and antioxidative nano zero-valent iron for the removal of hexavalent chromium. *Chemosphere* **262**, 127733 (2021).

41. Qiu, Y. *et al.* Removal mechanisms of Cr(VI) and Cr(III) by biochar supported nanosized zero-valent iron: Synergy of adsorption, reduction and transformation. *Environ. Pollut.* **265**, 115018 (2020).

42. Li, Y. *et al.* Hexavalent chromium removal from aqueous solution by adsorption on aluminum magnesium mixed hydroxide. *Water Res.* **43**, 3067–3075 (2009).

43. Barrera-Díaz, C. E., Lugo-Lugo, V. & Bilyeu, B. A review of chemical, electrochemical and biological methods for aqueous Cr(VI) reduction. *J. Hazard. Mater.* **223**–**224**, 1–12 (2012).

44. Marinho, B. A., Cristóvão, R. O., Boaventura, R. A. R. & Vilar, V. J. P. As(III) and Cr(VI) oxyanion removal from water by advanced oxidation/reduction processes—a review. *Environ. Sci. Pollut. Res.* **26**, 2203–2227 (2019).

45. Xu, C. *et al.* Performance and mechanism of Cr(VI) removal by zero-valent iron loaded onto expanded graphite. *J. Environ. Sci. (China)* **67**, 14–22 (2018).

46. Lv, D. *et al.* Mechanism and in fluence factors of chromium (VI) removal by sulfide-modified nanoscale zerovalent iron. *Chemosphere* **224**, 306–315 (2019).

47. Lv, X. *et al.* Nanoscale zero valent iron supported on MgAl-LDH-decorated reduced graphene oxide: Enhanced performance in Cr(VI) removal, mechanism and regeneration. *J. Hazard. Mater.* **373**, 176–186 (2019).

48. Azzam, A. M., El-Wakeel, S. T., Mostafa, B. B. & El-Shahat, M. F. Removal of Pb, Cd, Cu and Ni from aqueous solution using nano scale zero valent iron particles. *J. Environ. Chem. Eng.* **4**, 2196–2206 (2016).

49. Shao, F. *et al.* Detoxification of Cr(VI) using biochar-supported Cu/Fe bimetallic nanoparticles. *Desalin. Water Treat.* **158**, 121–129 (2019).

50. Fu, F., Cheng, Z. & Lu, J. Synthesis and use of bimetals and bimetal oxides in contaminants removal from water: a review. *RSC Adv.* **5**, 85395–85409 (2015).

51. Shi, L. na, Zhang, X. & Chen, Z. liang. Removal of Chromium (VI) from wastewater using bentonite-supported nanoscale zero-valent iron. *Water Res.* **45**, 886–892 (2011).

52. Yin, Y., Shen, C., Bi, X. & Li, T. Removal of hexavalent chromium from aqueous solution by fabricating novel heteroaggregates of montmorillonite microparticles with nanoscale zero-valent iron. *Sci. Rep.* **10**, 1–12 (2020).

53. Wang, C. *et al.* Comprehensive study on the removal of chromate from aqueous solution by synthesized kaolin supported nanoscale zero-valent iron. *Desalin. Water Treat.* **57**, 5065–5078 (2016).

54. Wang, Z. *et al.* Removal of hexavalent chromium by bentonite supported organosolv lignin-stabilized zero-valent iron nanoparticles from wastewater. *J. Clean. Prod.* **267**, 122009 (2020).

55. Li, S. *et al.* High dispersions of nano zero valent iron supported on biochar by one-step carbothermal synthesis and its application in chromate removal. *RSC Adv.* **9**, 12428–

12435 (2019).

56. Qian, L. *et al.* Nanoscale zero-valent iron supported by biochars produced at different temperatures: Synthesis mechanism and effect on Cr(VI) removal. *Environ. Pollut.* **223**, 153–160 (2017).

Authors contributions

M.B. designed and conducted the experiments, and wrote the manuscript. B.N. and C.F. supervised the whole study. All authors contributed in reviewing and editing the article and approved the final manuscript.

Figure legends:

Fig. 1. SEM images of (a) talc (b) Talc-nZVI/1Sn (c) Talc-nZVI/4Sn (d) Talc-nZVI/6Sn (e) Talc-nZVI/6Sn after reaction with Cr(VI)

Fig. 2. EDS mapping of the analyzed area; iron and tin in (a) Talc-nZVI/1Sn (b) Talc-nZVI/4Sn (c) fresh Talc-nZVI/6Sn and (d) Cr-treated Talc-nZVI/6Sn

Fig. 3. EDS spectra of (a) Talc-nZVI/6Sn and (b) Talc-nZVI/6Sn after reaction with Cr(VI)

Fig. 4. (a) FTIR spectra and (b) XRD patterns of Talc-nZVI/6Sn before and after Cr(VI) removal, (c) Zeta potential of Talc-nZVI/6Sn at different pH values

Fig. 5. Effect of (a) Sn/Fe ratio (b) adsorbent dosage (c) pH (d) temperature and (e) initial Cr(VI) concentration on Cr(VI) removal

Fig. 6. The effects of metallic cation's presence on the Cr(VI) removal using (a) Talc-nZVI/3Sn and (b) Talc-nZVI/6Sn (Cr(VI) initial concentration: 80 mg/L, metallic cations initial concentration: 40 mg/L, nanocomposite dosage: 1 g/L)

Fig. 7. (a) Aging study and (b) reusability of Talc-nZVI/6Sn

Fig. 8. (a) The variation of Cr concentration in aqueous solution (initial Cr(VI) concentration: 80 mg/L, temperature: 30 ℃, pH: 5, adsorbent dosage: 2 g/L) (b) Proposed mechanism of Cr(VI) removal by Talc-nZVI/6Sn

Table legends:

Table 1. solution pH before and after Cr(VI) removal

Table 2. Kinetic parameters for Cr(VI) removal by Talc-nZVI/6Sn

Table 3. Adsorption isotherm model parameters for Cr(VI) removal by Talc-nZVI/Sn

Table 4. Comparison of maximum removal capacity of Cr(VI) by supported-nZVI materials

Figures

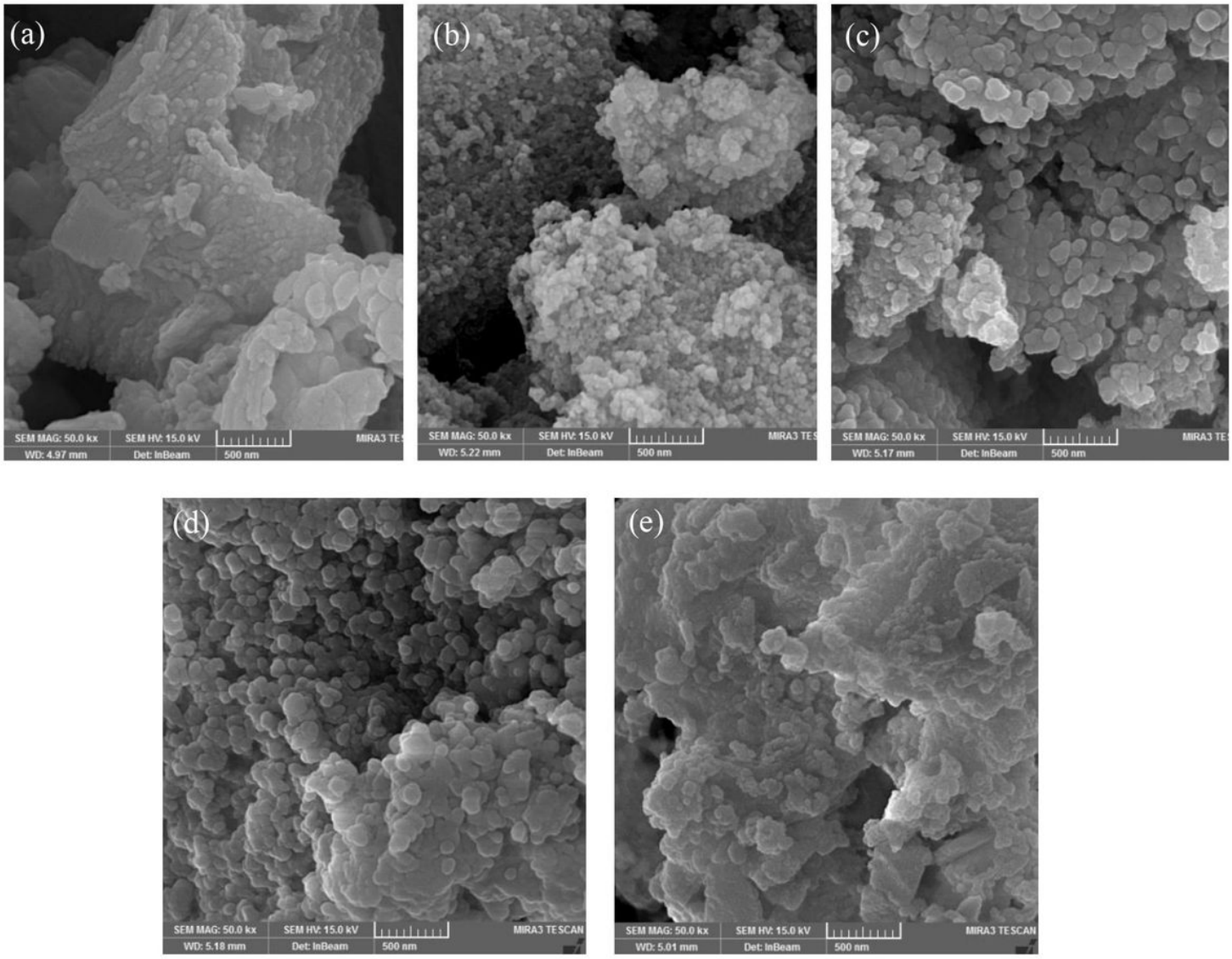

Figure 1

SEM images of (a) talc (b) Talc-nZVI/1Sn (c) Talc-nZVI/4Sn (d) Talc-nZVI/6Sn (e) Talc-nZVI/6Sn after reaction with Cr(VI)

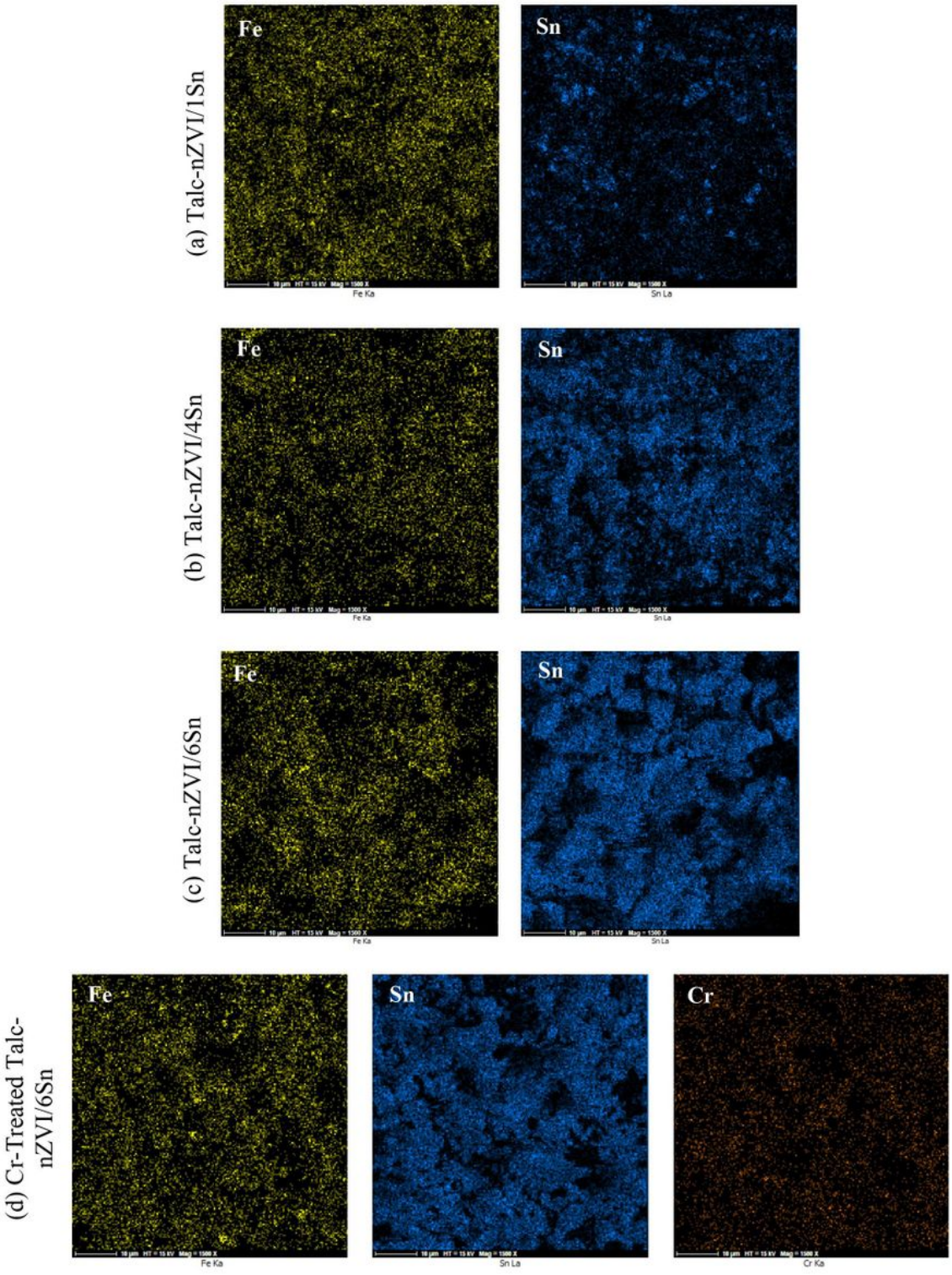

Figure 2

EDS mapping of the analyzed area; iron and tin in (a) Talc-nZVI/1Sn (b) Talc-nZVI/4Sn (c) fresh Talc-nZVI/6Sn and (d) Cr-treated Talc-nZVI/6Sn

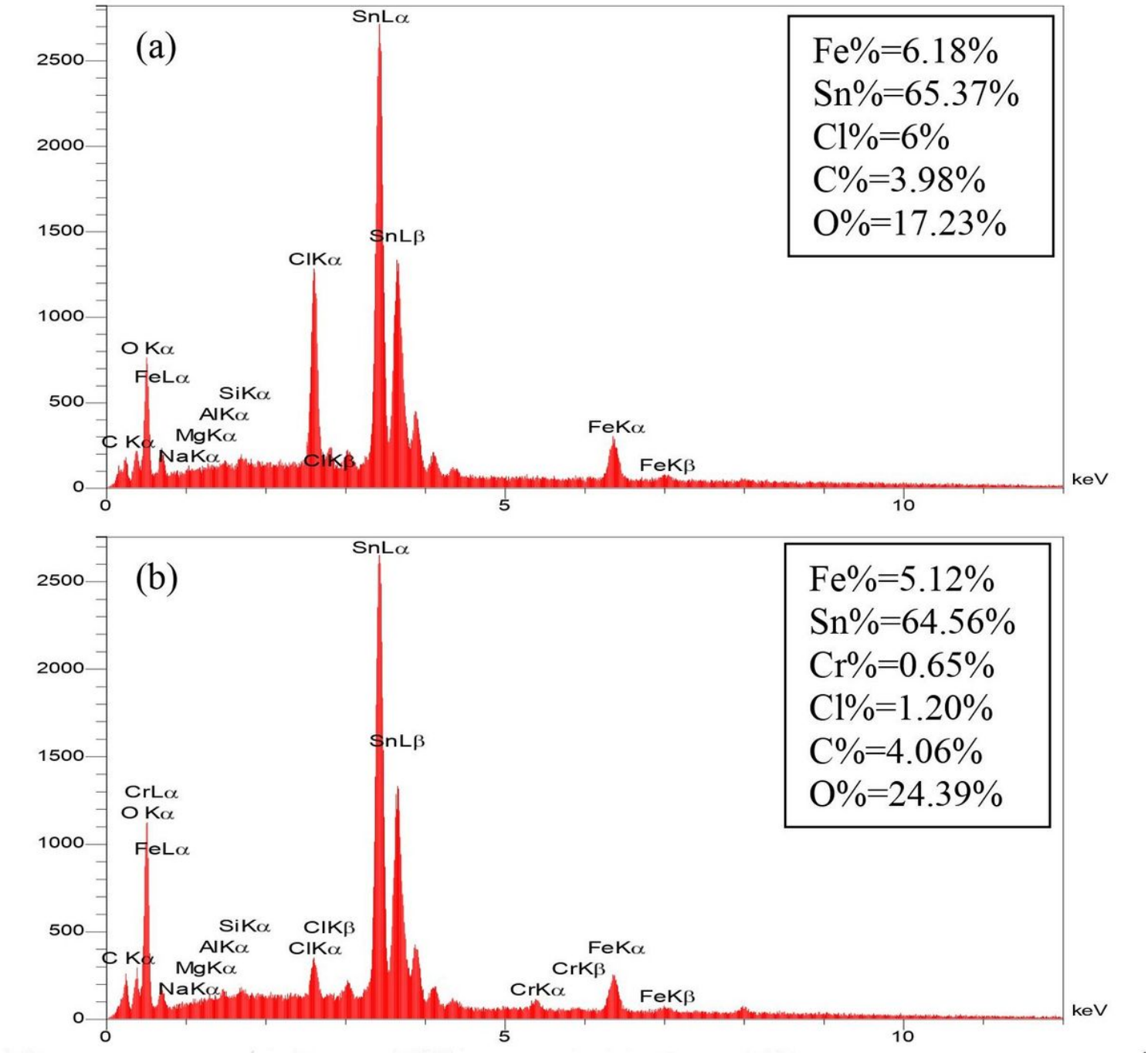

Figure 3

EDS spectra of (a) Talc-nZVI/6Sn and (b) Talc-nZVI/6Sn after reaction with Cr(VI)

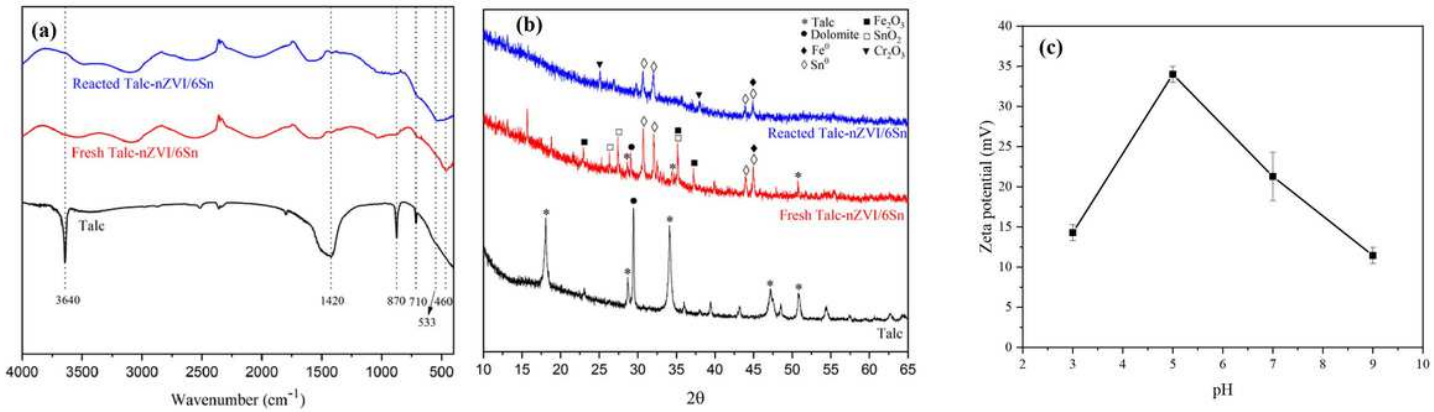

Figure 4

(a) FTIR spectra and (b) XRD patterns of Talc-nZVI/6Sn before and after Cr(VI) removal, (c) Zeta potential of Talc-nZVI/6Sn at different pH values

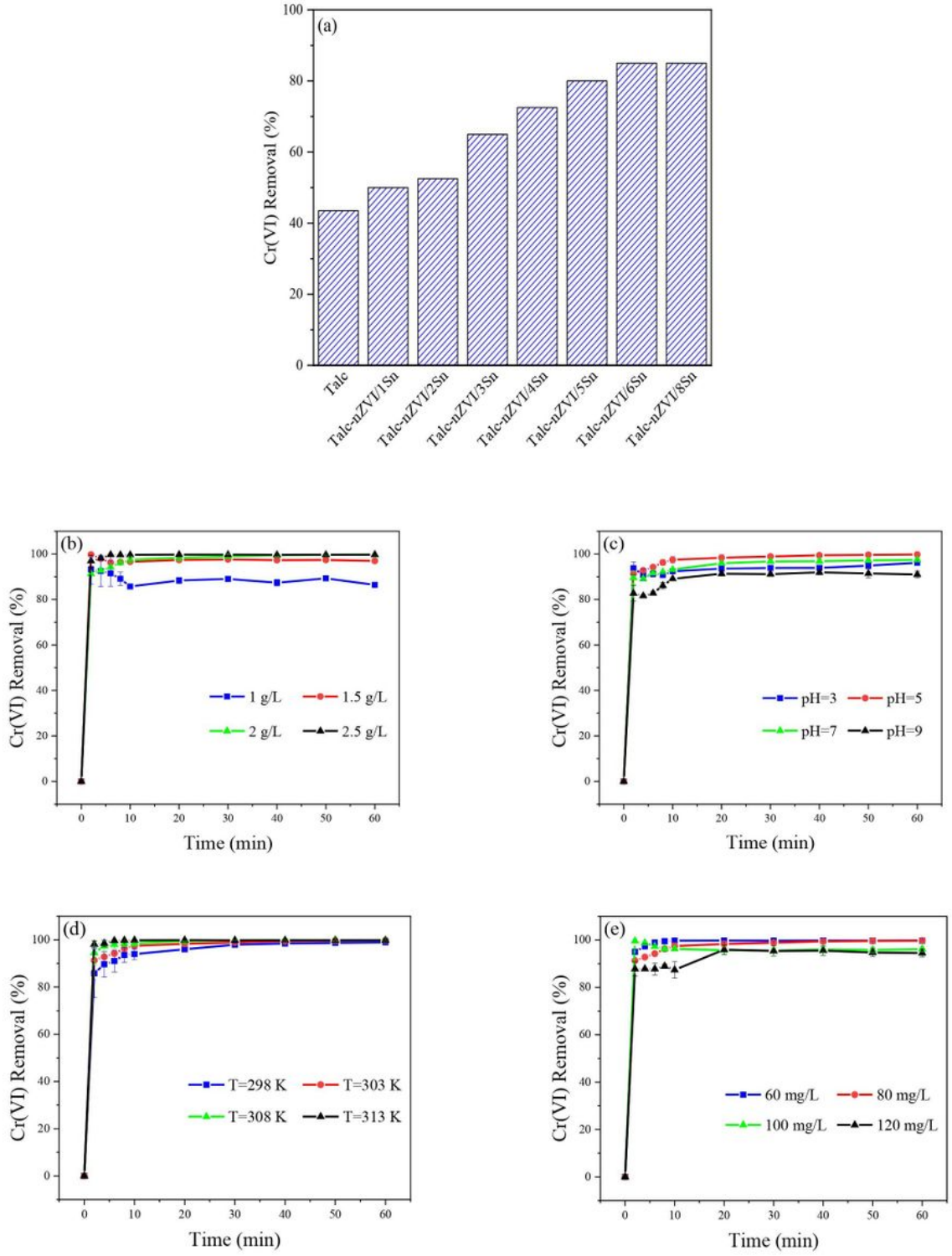

Figure 5

Effect of (a) Sn/Fe ratio (b) adsorbent dosage (c) pH (d) temperature and (e) initial Cr(VI) concentration on Cr(VI) removal

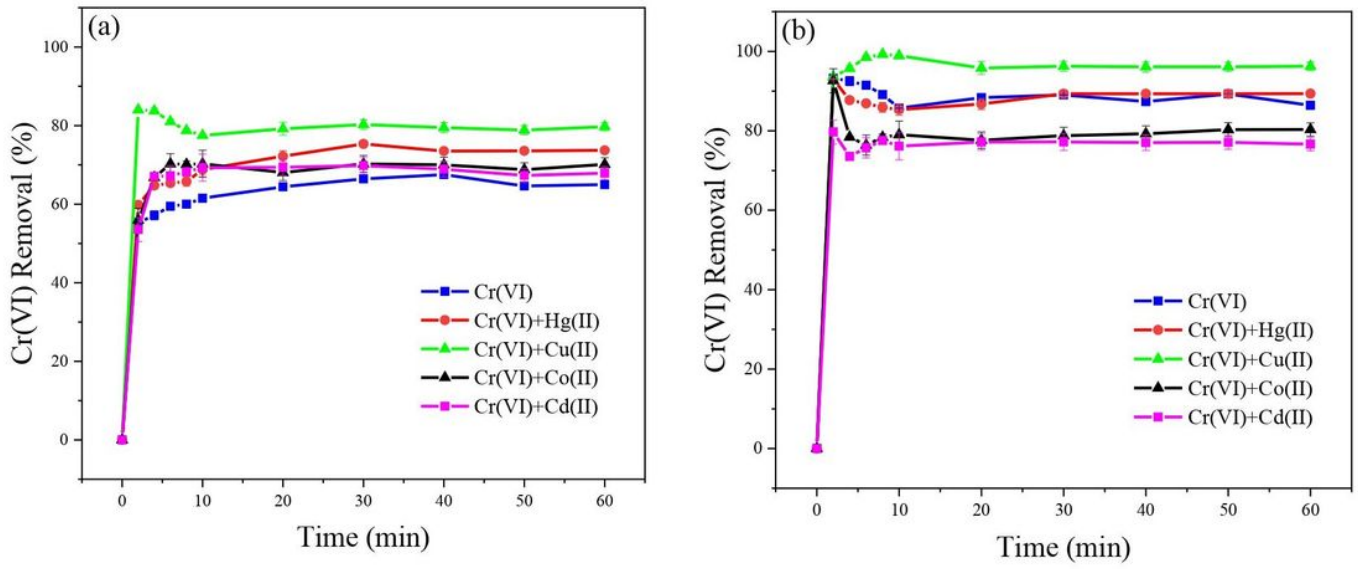

Figure 6

The effects of metallic cation's presence on the Cr(VI) removal using (a) Talc-nZVI/3Sn and (b) Talc-nZVI/6Sn (Cr(VI) initial concentration: 80 mg/L, metallic cations initial concentration: 40 mg/L, nanocomposite dosage: 1 g/L)

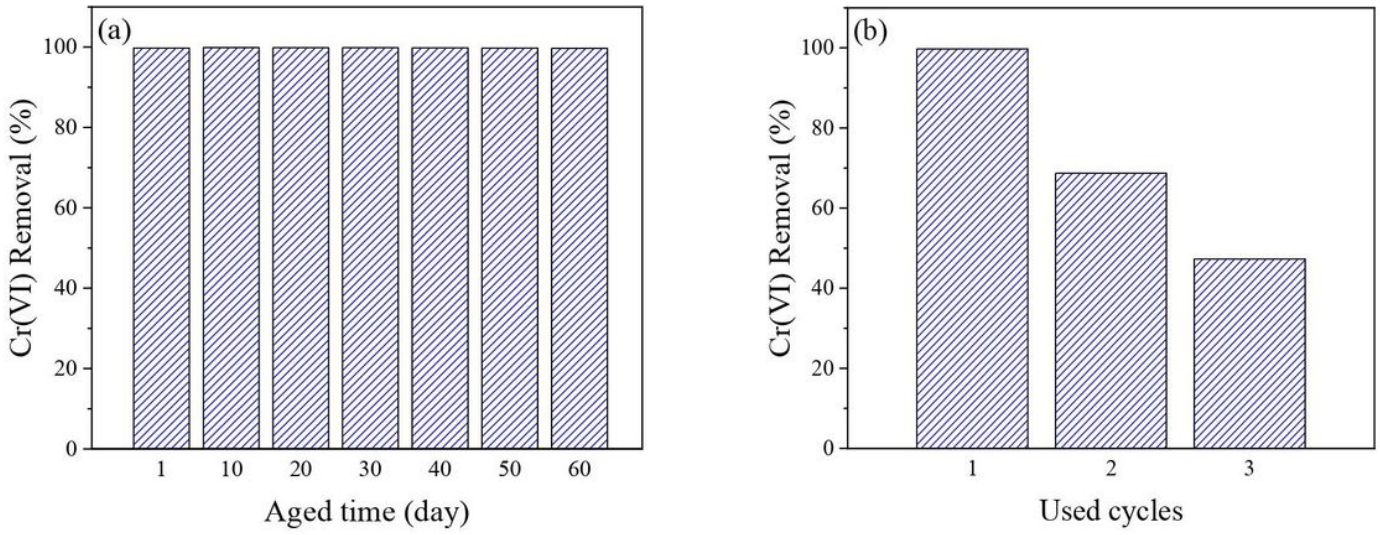

Figure 7

(a) Aging study and (b) reusability of Talc-nZVI/6Sn

Cr(VI) Removal Mechanism

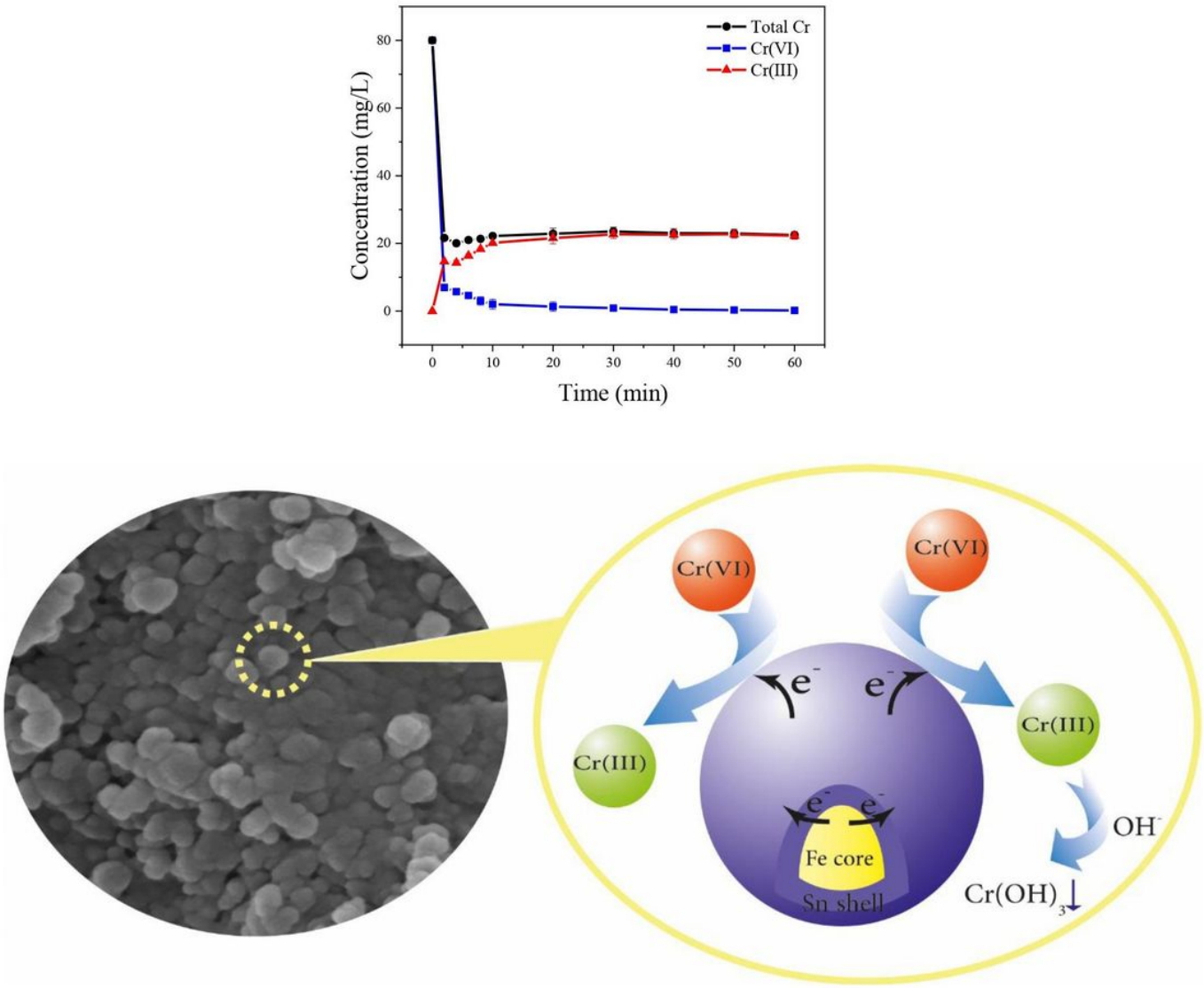

Figure 8

(a) The variation of Cr concentration in aqueous solution (initial Cr(VI) concentration: 80 mg/L, temperature: 30 □, pH: 5, adsorbent dosage: 2 g/L) (b) Proposed mechanism of Cr(VI) removal by Talc-nZVI/6Sn